



Gasdermin D Mediates a Mitochondrial Cell Death Pathway That Contributes to Pyroptosis.

Citation

Chang, Winston Yun-Han. 2019. Gasdermin D Mediates a Mitochondrial Cell Death Pathway That Contributes to Pyroptosis.. Master's thesis, Harvard Medical School.

Permanent link

<http://nrs.harvard.edu/urn-3:HUL.InstRepos:42057406>

Terms of Use

This article was downloaded from Harvard University's DASH repository, and is made available under the terms and conditions applicable to Other Posted Material, as set forth at <http://nrs.harvard.edu/urn-3:HUL.InstRepos:dash.current.terms-of-use#LAA>

Share Your Story

The Harvard community has made this article openly available.
Please share how this access benefits you. [Submit a story](#).

[Accessibility](#)

Gasdermin D Mediates a Mitochondrial Cell Death Pathway that Contributes to Pyroptosis.

Winston Yun-Han Chang

A Thesis Submitted to the Faculty of

The Harvard Medical School

in Partial Fulfillment of the Requirements

for the Degree of Master of Medical Sciences in Immunology

Harvard University

Boston, Massachusetts.

May 2019

Gasdermin D Mediates a Mitochondrial Cell Death Pathway that Contributes to Pyroptosis.

Abstract

Pyroptosis is an inflammatory cell death program triggered in innate immune cells by intracellular infections and sterile danger signals. The presence of intracellular DAMPs and PAMPs leads to inflammasome formation, inflammatory caspase activation and the cleavage of gasdermin D (GSDMD) into N-terminal (NT) and C-terminal fragments. GSDMD-NT forms pores on the plasma membrane, which release pro-inflammatory cytokines and cause cell death. We previously identified specific phospholipids to which GSDMD-NT binds, suggesting where pores may form during pyroptosis. Surprisingly, GSDMD-NT binds to and permeabilizes membranes containing cardiolipin, a phospholipid predominantly found on the inner mitochondrial membrane (IMM) and bacterial membranes. Studies suggest that cardiolipin can translocate to the outer mitochondrial membrane (OMM) through poorly defined mechanisms including mitochondrial scramblase PLS3, potentially becoming accessible to cytosolic GSDMD-NT. However, it remains unclear whether GSDMD-NT pores form on mitochondria, which may contribute to pyroptosis. Here, we demonstrate that GSDMD-NT permeabilizes mitochondria, leading to the release of mitochondrial proteins and DNA. Furthermore, GSDMD-NT permeabilization increases mitochondrial ROS production and reduces mitochondrial trans-membrane potential (MMP). In THP-1 cells undergoing NLRP3-mediated canonical pyroptosis GSDMD-NT localizes to mitochondria and releases mitochondrial proteins into the cytosol prior to permeabilization of the plasma membrane. Inhibition of cardiolipin synthesis and IMM-to-OMM translocation by siRNA knockdown of cardiolipin synthase (CLS) and PLS3, respectively, reduced pyroptosis. Based on these findings, we propose that GSDMD-NT mediates a mitochondrial pathway in pyroptosis which promotes cell death.

Table of Contents

| | |
|--|----|
| Chapter One: Background | 1 |
| 1.1 Inflammasomes and Pyroptosis | 1 |
| 1.2 Gasdermins | 5 |
| 1.3 Role of Pyroptosis in Disease | 6 |
| 1.4 GSDMD-NT Binds to Cardiolipin, a Mitochondrial Phospholipid | 7 |
| 1.5 Goal of Thesis | 13 |
| Chapter Two: Materials & Methods | 14 |
| Chapter Three: Results | 21 |
| Chapter Four: Discussion | 35 |
| Bibliography | 43 |
| Appendices | 48 |
| 6.1 Author Contributions | 48 |

List of Figures

Figure 1. The canonical and non-canonical pathway of pyroptosis.

Figure 2. GSDMD-NT binds to cardiolipin.

Figure 3. Cardiolipin biosynthesis in mammalian cells.

Figure 4. Cardiolipin externalization from IMM to OMM.

Figure 5. GSDMD-NT permeabilizes the OMM and IMM.

Figure 6. GSDMD-NT permeabilization of mitochondria leads to increased ROS production and reduced MMP.

Figure 7. GSDMD-NT localizes to mitochondria early in pyroptosis.

Figure 8. Cyt c is released from mitochondria during pyroptosis.

Figure 9. Caspase activation, GSDMD cleavage, and mitochondrial protein release are sequential.

Figure 10. Mitochondria are structurally damaged in pyroptotic cells.

Figure 11 Mitochondrial dysfunction and dissolution occur prior to plasma membrane permeabilization in individual pyroptotic cells.

Figure 12. Mitochondrial dysfunction precedes plasma membrane permeabilization in pyroptotic THP-1 cell populations.

Figure 13. Mitochondrial dysfunction precedes plasma membrane permeabilization in pyroptotic iBMDM populations.

Figure 14. siRNA knockdown of cardiolipin synthase or PLS3 scramblase attenuates pyroptosis.

Figure 15. GSDMD-NT mediates a mitochondrial cell death pathway that contributes to pyroptosis.

Acknowledgements

Firstly, I would like to thank Prof. Judy Lieberman for the opportunity to complete this thesis under her supervision. Her guidance, insights, and support have been invaluable towards the development and pursuit of our investigations.

I would also like to thank members of the Lieberman Lab, past and present, who have contributed to this thesis. Dr. Xing Liu made the early discoveries that sparked the thesis's hypothesis. Dr. Caroline Junqueira provided her imaging expertise to the study. Dr. Karla Mezza-Sosa, Dr. Sumit Sen-Santara, Dr. Zhibin Zhang, Dr. Angela Crespo, and Dr. Ying Zhang assisted in training. Dr. Tiewen Liu and Zhan Xu provided administrative and laboratory support. I would also like to recognize the collaboration with Prof. Hao Wu and her team, who provided materials for experiments conducted in this thesis.

The Master of Medical Sciences in Immunology program has also been supportive. I would like to thank the program directors, Prof. Shiv Pillai and Prof. Michael Carroll, for their guidance and feedback during the program. Thanks to Dr. Diane Lam and Dr. Gavin Porter for developing the program curriculum and providing learning experiences that aided in the thesis. I would also like to thank Selina Sarmiento for her administrative assistance.

Lastly, I would like to thank my family. Your hardships, never-ending support, and unconditional love have been the foundation of my educational journey thus far. The knowledge gained and accomplishments reached are shared with you.

This work was conducted with support from Students in the Master of Medical Sciences in Immunology program of Harvard Medical School. The content is solely the responsibility of the author and does not necessarily represent the official views of Harvard University and its affiliated academic health care centers

Chapter One: Background

1.1 Inflammasomes and Pyroptosis

The body is continuously in intimate contact with the microbial world. The host-microbial relationship is built upon the body's ability to facilitate peaceful interactions with commensals, while detecting and protecting itself from harmful pathogens. A key part of this ability lies in the barrier defense and early response of the innate immune system. To perform this task, barrier and tissue-resident sentinel cells possess a repertoire of toll-like receptors (TLRs) at the cell surface and within endocytic vesicles, which detect pathogen-associated molecular patterns (PAMPs). TLR binding to PAMPs, such as TLR4 to lipopolysaccharides (LPS) from gram-negative bacteria, results in the activation of interferon response pathways and master transcription factors NF- κ B and AP1. This leads to increased transcription of sensor, adaptor and effector proteins that enhance PAMP and danger-associated molecular pattern (DAMP) recognition to help innate immune cells tailor responses towards a pathogen. These transcripts include diverse cytosolic receptors such as RIG-I and cGAS/STING, which detect foreign nucleotides and induce an anti-infection interferon response. Other cytosolic receptors such as NOD-like receptors (NLRs), AIM2-like receptors (ALRs) and pyrin detect pathogenic antigens and cell stressors—flagellin, toxins, dsDNA, ATP and ROS. After sensing their targets, certain cytosolic receptors (NLRP1, NLRP3, NAIP, AIM2 and pyrin) interact with adaptor proteins ASC or NLRC4 to form supramolecular organizing centers (SMOCs) called inflammasomes (1). Inflammasomes initiate molecular pathways within innate immune cells that lead to pyroptosis, an inflammatory cell death program.

Pyroptosis was originally identified in macrophages that were infected with the invasive intracellular pathogens *Shigella flexneri* and *Salmonella typhimurium* (2-5). Although pyroptosis causes late-stage caspase-3 activation and membrane blebbing like non-inflammatory apoptosis, early mechanistic investigations determined that the death of these macrophages was uniquely caspase-1-dependent (2, 6-

11). Furthermore, pyroptosis was a much faster cell death program than apoptosis, causing population-wide cell death in less than an hour (12, 13). Death of infected macrophages resulted in the release of pro-inflammatory cytokines independently of the RIPK3-MLKL mechanism of necroptosis, another inflammatory cell death program. Under microscopy, pyroptotic cell morphology differs from apoptosis and necroptosis. Unlike the swelling and violent bursting in necroptosis, pyroptotic cells possess permeabilized membranes and osmotic balance that facilitate gradual flattening of cells as inflammatory intracellular content is released (14-16).

In innate immune cells, pyroptosis occurs through two pathways—the canonical and non-canonical (17, 18) (Fig. 1). In the canonical pathway, inflammasomes recruit pro-caspase-1, which is auto-proteolyzed to become active. Caspase-1 cleaves cytosolic proteins, including the inactive precursor of pro-inflammatory cytokines, IL-1 β and IL-18, which are transcriptionally upregulated in response to TLR signaling. While caspase-1 cleavage generates active cytokines, these inflammatory mediators require a mechanism for extracellular release, since they lack a secretion signal. Another important caspase-1 target is the cytosolic protein gasdermin D (GSDMD). Caspase-1 cleavage separates GSDMD into N- and C-terminal fragments. The N-terminal fragment of GSDMD (GSDMD-NT) is a membrane-pore-forming protein, which targets the plasma membrane. Pore formation leads to loss of cell membrane integrity, the hallmark of pyroptosis, and mediates the release of active IL-1 β and IL-18 from the cytosol. GSDMD-NT is also responsible for eventual cell death. The non-canonical pathway differs in the inflammatory caspases utilized, and their method of activation. In the presence of intracellular LPS, inflammatory caspase-11 (mice) or caspase-4/5 (human) directly bind LPS and become activated independently of any other molecules. Caspase-4/5/11 then cleave GSDMD to generate GSDMD-NT, which permeabilizes the plasma membrane. Caspase-4/5/11 do not cleave precursor IL-1 β and IL-18 like caspase-1. However, active pro-inflammatory cytokine release through GSDMD-NT pores occurs in the non-canonical pathway due to

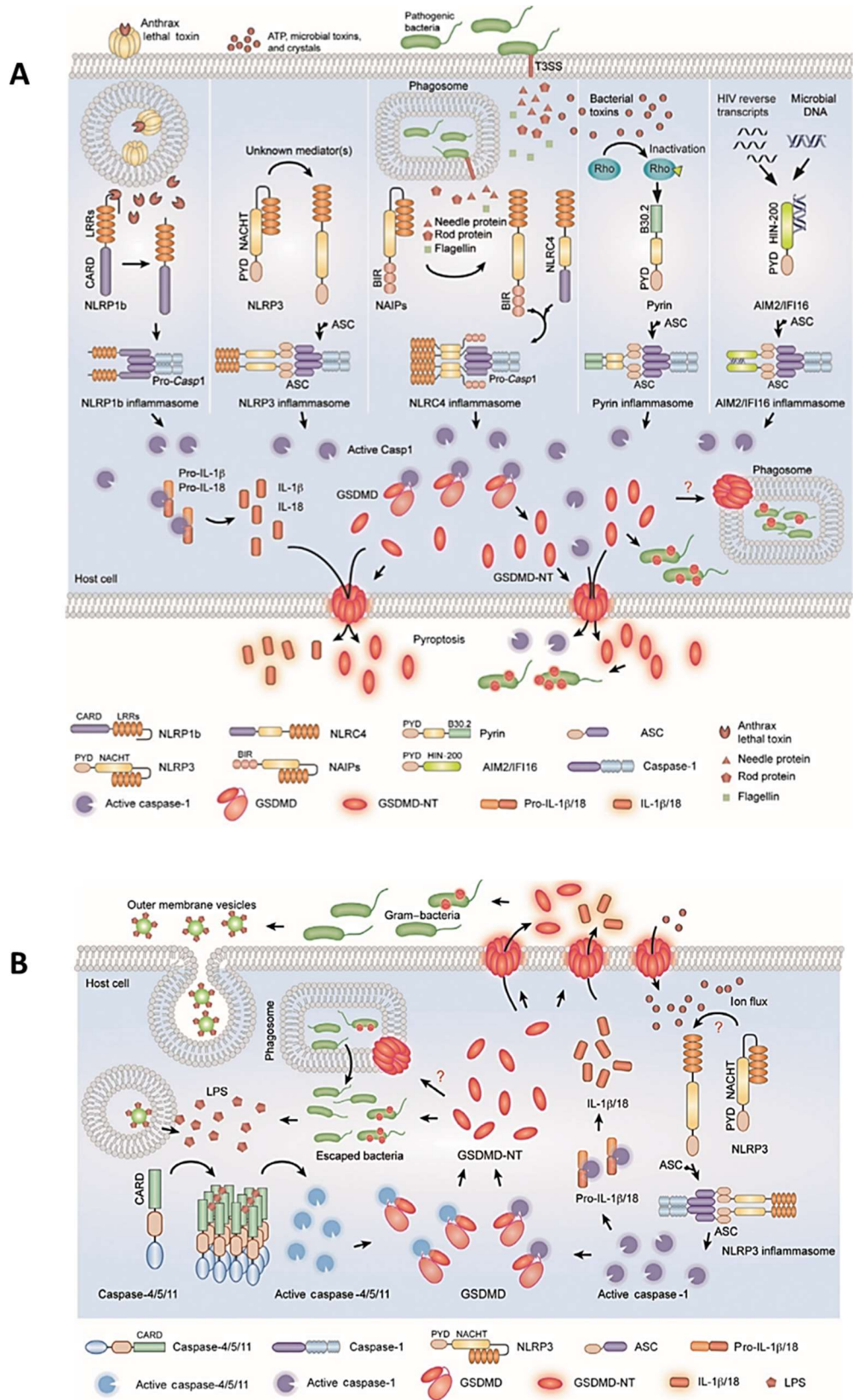


(Figure 1. See figure legend on next page)

Figure 1. The canonical and non-canonical pathway of pyroptosis. (A) The canonical pathway is activated by a diverse repertoire of cytosolic receptors. NLR proteins (NLRP1, NLRP3, NAIP/NLRC4), pyrin and ALR proteins (AIM2 and IFI16) sense danger signs and initiate assembly of canonical inflammasomes. NLRP1 is activated by the metalloprotease activity of *Bacillus anthracis* lethal toxin (LT). The NLRP3 inflammasome is activated by a broad spectrum of stimuli, such as ATP, microbial toxins, and crystals. NAIPs recognize and directly bind to bacterial flagellin or bacterial type III secretion system components to initiate the NLRC4 dependent inflammasome. Pyrin detects the inactivation of Rho GTPases by bacterial toxins. AIM2 and IFI16 sense dsDNA. The canonical inflammasome complexes form a platform to activate caspase-1. Activated caspase-1 processes pro-inflammatory cytokine precursors (pro-IL-1 β , pro-IL-18) and cleaves GSDMD, releasing its N-terminal fragment GSDMD-NT, which forms pores in the plasma membrane of the infected cell, resulting in cytokine release and cell death. (B) In the non-canonical pathway, cytosolic LPS from intracellular gram-negative bacteria binds to caspase4/5/11, causing self-assembly of the non-canonical inflammasome. These caspases are then activated and trigger pyroptosis by cleaving GSDMD. Active caspase-4/5/11 do not directly cleave the proinflammatory cytokine precursors but cause them to be processed indirectly by secondary activation of the NLRP3 inflammasome and caspase-1. Figure adapted from Liu & Lieberman (18).

secondary activation of the NLRP3 canonical pathway by cell membrane damage (17). Pro-inflammatory cytokines may also be released through poorly-defined GSDMD-NT-independent pathways during pyroptosis (19).

1.2 Gasdermins

GSDMD plays a central role as the effector of pyroptosis in innate immunity. The protein's role in pyroptosis was highlighted by early proteomic studies indicating GSDMD as a substrate of inflammatory caspases (20). Later studies validated GSDMD's role in pyroptosis as *Gsdmd*^{-/-} immortalized bone marrow-derived macrophages (iBMDMs) no longer released cytokines and died in response to non-canonical LPS transfection and had a delayed response to canonical inflammasome stimuli. This suggested a critical role for GSDMD in executing pyroptosis, but indicated the presence of alternative caspase-1-dependent pathways (12, 13). Although GSDMD's role in pyroptosis became clearer, how it caused pyroptosis was uncertain. GSDMD is expressed as a full length ~50 kDa protein that is cleaved by inflammatory caspases-1/4/5/11 after Asp275/276 (human/mouse) to generate a ~30 kDa N-terminal fragment (GSDMD-NT). Mutation of the cleavage residue prevents pyroptosis (12). Analysis of GSDMD-NT's predicted structure noted homology to the membrane attack domain of perforin, a membrane pore-forming protein involved in immune cell-mediated killing. This led researchers to postulate that GSDMD-NT acts as an oligomerizing membrane-pore-forming protein (15, 21-24). When liposomes containing phosphatidylinositol phosphates were treated with GSDMD-NT, their internal content was released, suggesting membrane permeabilization. Furthermore, when GSDMD-NT was electrophoresed in Western blots using non-reducing gels, the protein appeared at a higher molecular weight than 30 kDa. In a reducing gel however, GSDMD-NT appears at the appropriate protein size for the monomer, confirming oligomerization of GSDMD-NT. The separation of GSDMD-NT monomers under reducing conditions suggested that oligomerization occurs through intermolecular cysteine interactions. Indeed, mutations of Cys39 and Cys192 residues in GSDMD-NT

prevented oligomerization. Ultimately, negative-stain electron microscopy (EM) identified pore structures on liposomes, solidifying the molecular function of GSDMD-NT as a membrane pore-forming protein (24).

The identification of the GSDMD-NT pore encouraged researchers to define its structure—a challenging endeavor given difficulties with recombinant protein aggregation. As a result, structural details of GSDMD-NT pores have been inferred from homologous gasdermin family members. In humans, the gasdermin family is composed of four members, GSDMA, GSDMB, GSDMC and GSDMD. In addition, there is a closely related pejkakin family, containing DFNA5/GSDME and DFNB59, that share homology within their N-terminal domain. The mouse genome also encodes for gasdermins, that include duplicates of GSDMA and GSDMC (GSDMA1-3, GSDMC1-4). The gasdermin family, members share strongly conserved NT and CT domains, but vary in the linking region where cleavage occurs (18). Most structural studies have focused on gasdermin A3 (GSDMA3). A recent cryo-EM structure of the GSDMDA3 pore suggests that GSDMA3-NTs undergo dramatic conformational changes to assemble into a pore. The α 1 helix of GSDMA3 binds to acidic phospholipids during membrane insertion. Oligomerization of monomers is mediated by membrane-embedded beta-sheets and associated globular domains. Twenty-seven monomers form a pore that is 180 Å in diameter, with hydrophobic residues facing the lipid bilayer and hydrophilic residues facing the pore channel (25).

1.3 Role of Pyroptosis in Disease

Pyroptosis has important effects on human health and disease. Pyroptotic death of innate immune cells and barrier cells compromises intracellular niches of pathogens, making them more susceptible to other immune components. Furthermore, the inflammation generated by pyroptosis strengthens innate immunity and kickstarts adaptive immunity. Release of IL-1 β by macrophages induces endothelial cell expression of chemokines, selectins and integrins responsible for leukocyte extravasation, activates the acute phase protein response, and promotes T cell and B cell activation. Genetic deficiency of the NLRP3

inflammasome in colonic epithelial cells leads to overgrowth of certain gut bacterial species and increases predisposition to inflammatory bowel disease (26). Furthermore, *Casp11*^{-/-} mice have higher susceptibility to microbiota-induced colitis (27). While pyroptosis is protective in healthy individuals, the strength and timing of pyroptosis must be carefully controlled. In disseminated infection, intense and prolonged pyroptosis can cause chronic inflammation that results in sepsis. Severe inflammation leads to vascular leakage, multi-organ failure, septic shock and death. In *in vivo* studies of LPS challenge that model sepsis, *Gsdmd*^{-/-} mice survive (12). While LPS injections in mice usually trigger sepsis and mortality, the absence of GSDMD protects these mice. Clinically, sepsis remains a serious challenge. Sepsis is the leading cause of global child mortality and is associated with 30% of hospitalized deaths in the United States (18). However, therapeutic strategies to treat sepsis, other than antibiotics, remain elusive. Neutralization of pro-inflammatory cytokines has not improved clinical outcomes and supportive care remains the primary approach. Even if a patient recovers from sepsis, complications lead to a significantly reduced lifespan. Given the link between pyroptosis and sepsis, a better understanding of pyroptosis and its molecular pathways may provide novel therapeutic approaches.

1.4 GSDMD-NT Binds to Cardiolipin, a Mitochondrial Phospholipid

Our laboratory and a team led by Dr. Feng Shao, have previously investigated the lipid specificity of GSDMD-NT's membrane attack domain. GSDMD-NT binds to acidic phospholipids, such as phosphatidic acid, phosphatidylserine and phosphatidylinositol predominantly found on the inner leaflet of the plasma membrane. This leads to plasma membrane pore formation from within the cell. GSDMD-NT also has greater affinity for cardiolipin, a phospholipid found on the inner mitochondrial membrane (IMM) and bacterial membranes (24) (Fig. 2).

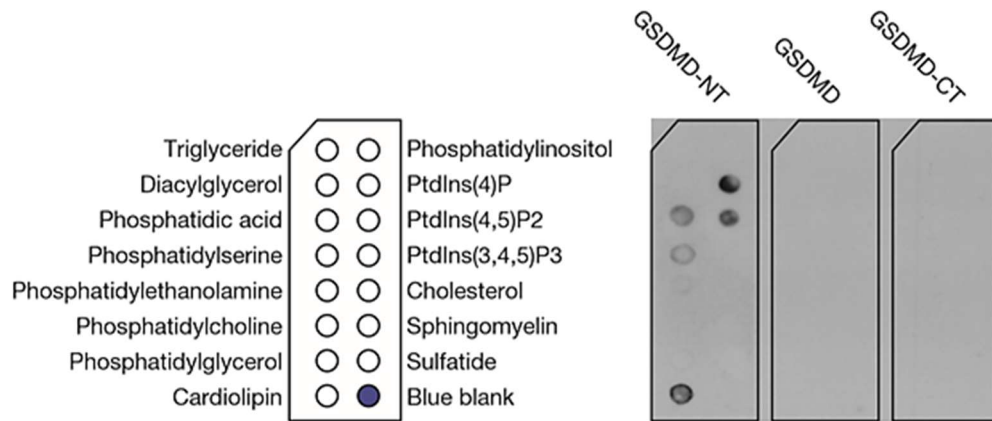


Figure 2. GSDMD-NT binds to cardiolipin. Membrane strips dotted with phospholipids were incubated with GSDMD-NT, GSDMD-CT or full-length GSDMD and protein binding was assessed by blotting. Results demonstrate that only GSDMD-NT can bind lipids. GSDMD-NT binds to anionic phospholipids found in the inner-leaflet of the plasma membrane and cardiolipin, a phospholipid in mitochondrial and bacterial membranes. Figure taken from Liu *et al.* (24).

Cardiolipin is a negatively charged phosphatidylglycerol lipid that in eukaryotic cells, is synthesized in the mitochondrial matrix (Fig. 3). Phosphatidic acids synthesized at the outer mitochondrial membrane (OMM) and endoplasmic reticulum are shuttled to the matrix, where they are processed by proteins bound to the matrix-facing leaflet of the IMM (28-32). Here phosphatidic acids are converted to cytidine diphosphate-diacylglycerol (CDP-DAG) through a reaction with cytidine triphosphate, which is catalyzed by the CDP-DAG synthase TAMM41 (33-35). Commitment to cardiolipin synthesis occurs with the conversion of CDP-DAG to phosphatidylglycerol phosphate (PGP) by PGP synthase (36). PGP is dephosphorylated by PTPM1 to phosphatidylglycerol (PG), which condenses with another CDP-DAG to form cardiolipin. This last synthesis step is catalyzed by cardiolipin synthase (CLS) (37-40). Given its unique location in mitochondria, it is no surprise that cardiolipin has important organelle-specific roles. Cardiolipin contributes to the negative charge of the IMM, which attracts protons in the mitochondrial intermembrane space (IMS) that are needed for ATP synthase (41). Cardiolipin also stabilizes oxidative phosphorylation components and mediates assembly of respiratory complexes responsible for electron transfer. This minimizes ROS leakage from the IMM electron transport chain (42-49). Mitochondrial membrane fission/fusion and the assembly of ATP synthase subunits is also mediated by cardiolipin. The importance of cardiolipin is demonstrated by organelle dysfunction and loss of cell viability when CLS is inhibited (50).

While cardiolipin is enriched at the IMM, it also externalizes to the OMM (Fig. 4). Several mechanisms have been proposed to mediate cardiolipin's movement from the IMM to OMM. One mechanism involves the mitochondrial inner and outer membrane contact sites (MICOS), which create the organelle's cristae. MICOS are crucial for transporting molecules needed for mitochondrial biosynthesis and energy for cellular functions. These contact sites contain proteins that bind and potentially externalize cardiolipin to the OMM (51, 52). The most well-studied externalization mechanism involves PLS3, a calcium-dependent mitochondrial scramblase. Like other scramblases, PLS3 mediates the symmetrical distribution

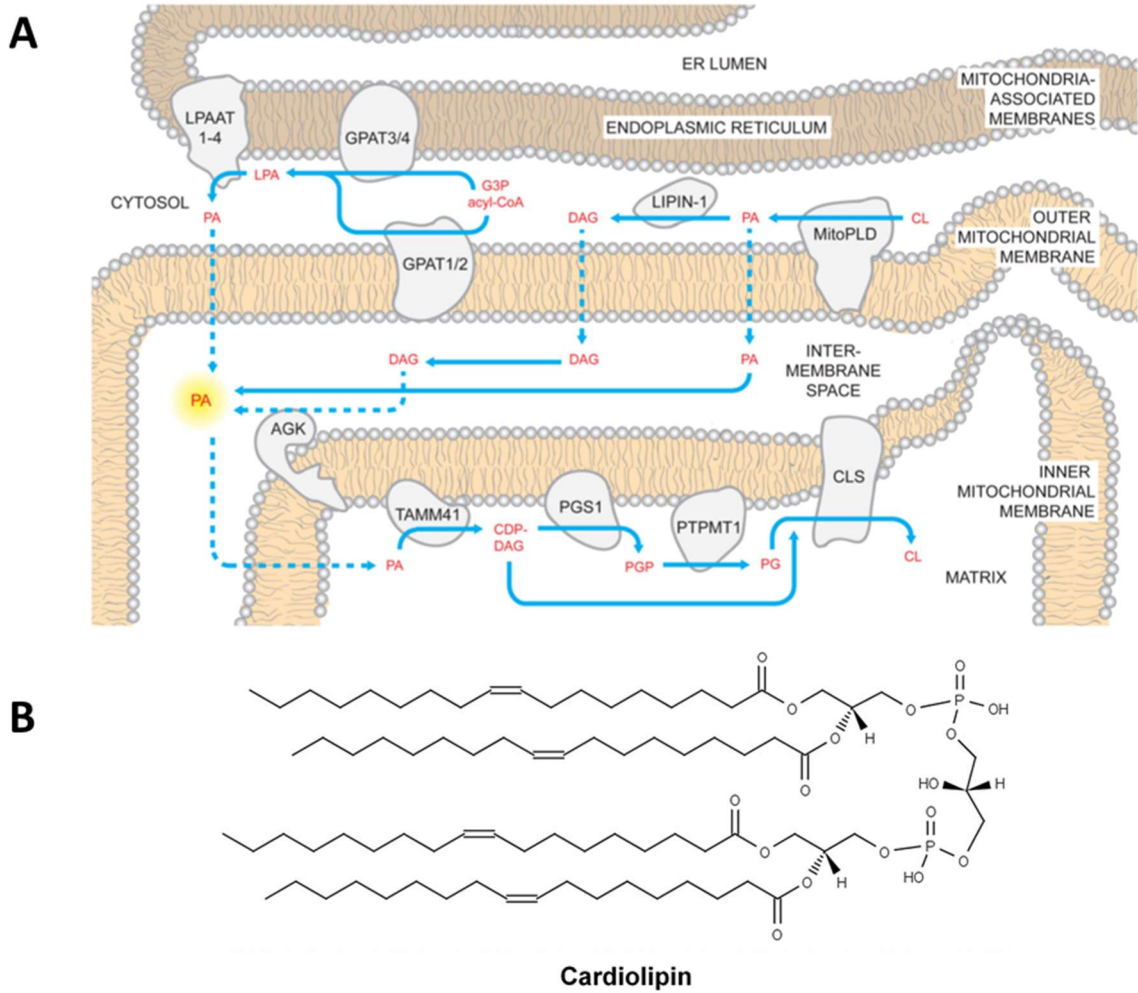


Figure 3. Cardiolipin biosynthesis in mammalian cells. (A) Cardiolipin biosynthesis begins with the shuttling of phosphatidic acid (PA) from multiple sources to the mitochondrial matrix. In the matrix, PA gains access to the core cardiolipin synthesis machinery. PA is converted to cytidine diphosphate-diacylglycerol (CDP-DAG) by TMM41. Commitment to cardiolipin synthesis occurs when CDP-DAG is converted to phosphatidylglycerol phosphate (PGP) by PGP synthase (PGS1). PGP is rapidly dephosphorylated by mitochondrial protein tyrosine phosphatase, PTPMT1, and the phosphatidylglycerol (PG) produced is condensed with another CDP-DAG by cardiolipin synthase (CLS) to generate cardiolipin (CL). (B) Chemical structure of cardiolipin. Figure adapted from Lu & Claypool (50).

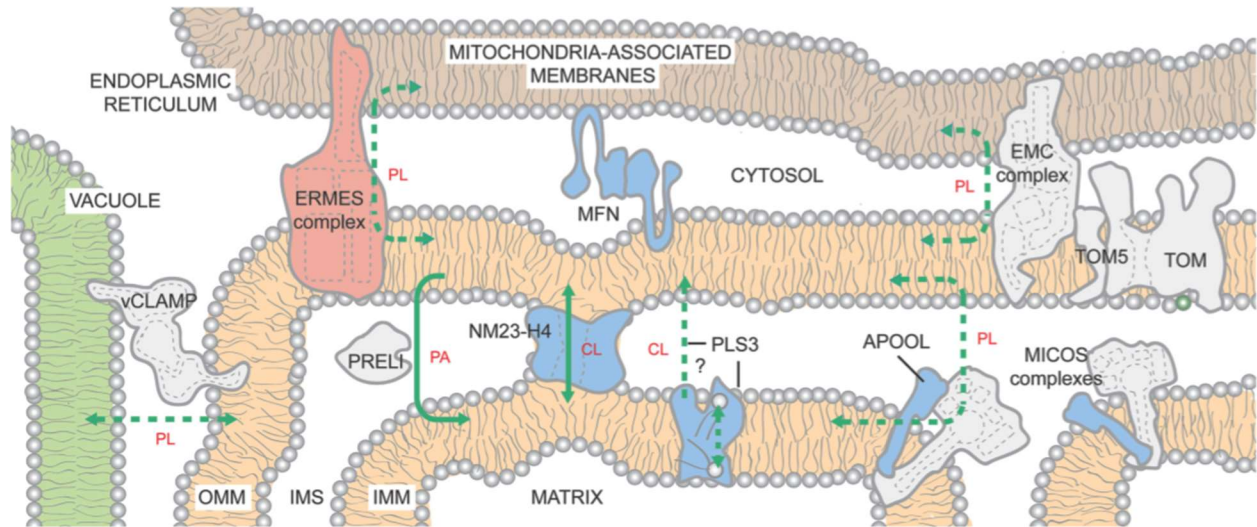


Figure 4. Cardiolipin externalization from IMM to OMM. Within the mitochondrion, cardiolipin (CL) trafficking between IMM and OMM may involve contact sites between the OMM and the IMM (MICOS) or the general anionic phospholipid transporter NM23-H4. The mitochondrial scramblase, PLS3, also contributes to externalizing cardiolipin to the OMM. However, it is unclear whether PLS3 directly transports cardiolipin from the IMM to the OMM or redistributes cardiolipin between both leaflets of the IMM for transport by other mechanisms. Figure taken from Lu & Claypool (50).

of phospholipids across lipid bilayers, in this case, from the matrix to the IMS-facing leaflet of the IMM (53-55). However, overexpression of PLS3 also increases cardiolipin externalization to the OMM, potentially involving additional mitochondrial components (55, 56). Another proposed mechanism involves a general anionic phospholipid transferase, NM23-H4/NDPK-D, that shuttles between the IMM and OMM (57). Although cardiolipin OMM externalization occurs during cell homeostasis, it increases dramatically during mitochondrial stress and damage. In fact, high levels of OMM cardiolipin trigger mitophagy and promote the mitochondrial pathway of apoptosis. The increasing negative charge of the OMM due to cardiolipin externalization attracts and stabilizes the insertion of pro-apoptotic Bax/Bad, which permeabilize the OMM (58, 59). Furthermore, OMM cardiolipin promotes caspase-8 recruitment to mitochondria, where it can become activated to generate the OMM-permeabilizing protein t-BiD (60).

Permeabilization of the OMM leads to the cytosolic release of molecules from the organelle that mediate the mitochondrial pathway of apoptosis. Soluble IMS proteins such as cytochrome C (Cyt c) and Htra2/Omi play important roles when released into the cytosol. Cyt c interacts with the adaptor protein APAF-1 to form a SMOC called the apoptosome. Pro-caspase-9 is recruited to the apoptosome, where it is autocatalyzed to the active form. Caspase-9 then cleaves pro-caspase-3 to caspase-3, which serves as the executioner protease for apoptosis. OMM permeabilization also triggers autocatalyzed activation of Htra2, a protease that degrades inhibitors of apoptotic proteases (IAPs) that usually block caspase-3/7/9 activation, thus promoting apoptosis (61). Recent studies have also demonstrated that OMM permeabilization by Bax/Bad releases mitochondrial DNA (mtDNA) into the cytosol (62). Permeabilization of the OMM during apoptosis ultimately results in disruption of cristae structure, increased ROS production, and loss of mitochondrial trans-membrane potential (MMP) (63).

1.5 Goal of Thesis

Given GSDMD-NT's affinity for cardiolipin, we reasoned that GSDMD-NT pore formation might occur at mitochondria. Permeabilization of mitochondrial membranes by GSDMD-NT could lead to the release of mitochondrial molecules and cause mitochondrial dysfunction. GSDMD-NT's disruption of mitochondria would likely trigger downstream molecular pathways which could contribute to pyroptotic cell death. Taken together, we hypothesized that GSDMD-NT could trigger a mitochondrial cell death pathway that contributes to pyroptosis. Testing this hypothesis is the goal of this thesis.

Chapter Two: Materials and Methods

Cell Culture

HCT116 cells (5×10^6 cells) were seeded in 150 mm culture dishes and cultured for 2-3 days in complete medium (DMEM, 10% FBS, 100 U/mL penicillin G, 100 $\mu\text{g}/\text{mL}$ streptomycin sulfate, 6 mM HEPES, 1.6 mM L-glutamine, 50 μM 2-mercaptoethanol) and used when 80% confluent.

THP-1 cells (5×10^5 cells/mL) were seeded in 75 mm² culture flasks and cultured for 3 days in complete medium (RPMI-1640, 10% FBS, 100 U/mL penicillin G, 100 $\mu\text{g}/\text{mL}$ streptomycin sulfate, 6 mM HEPES, 1.6 mM L-glutamine, 50 μM 2-mercaptoethanol). To differentiate THP-1 cells into adherent macrophages, cells were activated with PMA (50 ng/mL) for 36-48 hrs. To induce pyroptosis, THP-1 macrophages were primed with LPS (1 $\mu\text{g}/\text{mL}$, 4 hrs), followed by treatment with nigericin (20 μM ; InvivoGen, tlr1-nig).

Murine immortalized bone-marrow derived macrophages (iBMDMs; a gift from Dr. Jon Kagan) (5×10^6 cells) were seeded in 150 mm culture dishes and cultured for 2 days in complete medium (DMEM, 10% FBS, 100 U/mL penicillin G, 100 $\mu\text{g}/\text{mL}$ streptomycin sulfate, 6 mM HEPES, 1.6 mM L-glutamine, 50 μM 2-mercaptoethanol) and used when 80% confluent. To induce pyroptosis, iBMDMs were primed with LPS (1 $\mu\text{g}/\text{mL}$, 4 hrs) and treated with either nigericin (20 μM) or ATP (5 mM).

Isolation and Treatment of Mitochondria

7.5×10^7 HCT116 cells were washed and collected in PBS with gentle scraping. Cells were centrifuged (400 xg, 4°C, 10 min), resuspended in 5 times volume of isotonic Buffer A (10 mM Tris-Cl pH 7.5, 10 mM KCl, 250 mM sucrose, 1.5 mM MgCl_2) and incubated at 4°C for 15 min. Cells were then homogenized using a glass homogenizer, applying 30 strokes. Homogenate was centrifuged (1000 xg, 4°C,

10 min) to pellet nuclei. The post nuclear supernatant was collected and centrifuged (7000 xg, 4°C, 10 min) to collect mitochondria. The mitochondria pellet was resuspended in 2 times volume of Buffer A.

Isolated mitochondria were treated with recombinant human GSDMD (5 µM) and caspase-11 (5 µM), provided by Dr. Hao Wu, and incubated for indicated times at 37°C with shaking. Control mitochondria were also treated with recombinant mouse t-BID (7.5 µg/mL; Prospec; pro-644). The pan-caspase inhibitor Z-VAD-FMK (5 µM; BD Pharmogen, 550377) was also used in indicated samples. After treatment mitochondria were pelleted by centrifugation (18,500 xg, 4°C, 20 min), and the post-treatment supernatant was collected. The pelleted mitochondria were lysed (50 mM Tris-Cl pH7.5, 150 mM NaCl, 1 mM EDTA, 1% Triton X-100,) at 4°C for 15 min, followed by centrifugation (18,500 xg, 4°C, 20 min).

Western Blots

Samples were boiled in SDS loading buffer (85°C, 5 min), and then electrophoresed through 15% SDS-PAGE gels. Resolved proteins were transferred to a polyvinylidene difluoride (PVDF) membrane (Millipore). Membranes were blocked (2% milk, 0.05% Tween-20, in TBS; 1 hr, RT) before being probed with the following primary antibodies (4°C, overnight): COX IV (Cell Signaling Technology, 4950S; 1:1000), cytochrome c (Cyt c) (BioLegend, 612504; 1:500), HtrA2/Omi (Cell Signaling Technology, 9745S; 1:1000), superoxide dismutase 2 (SOD2) (Santa Cruz Biotechnology, SC-30080; 1:1000), aconitase 2 (ACO2) (Cell Signaling Technology, 6571T; 1:1000), IL-1β (R&D Systems, AF-2010NA; 1:1000), cleaved caspase-1 (Cell Signaling Technologies, 4199S; 1:500), caspase-3 (Cell Signaling Technologies, 9662S; 1:500), GSDMD (lab generated, 1:500), α-tubulin (Sigma-Aldrich, T5168; 1:500). Membranes were washed three times for 10 min in TBS-T (0.05% Tween-20 in TBS), before incubation with HRP-tagged secondary antibodies (GE Healthcare, NA931V & NA934V; Invitrogen, 61-1620; 1:5000, 1 hr, RT). After washing, bound antibodies were detected using SuperSignal West Femto Maximum Sensitivity Substrate (Thermo Fisher, 34095) and a ChemiDoc MP Imaging System (BioRad).

Mitochondrial DNA Release Assay

DNA was extracted from samples using the DNeasy Blood & Tissue Kit (Quagen) according to supplier instructions. MtDNA was quantified by qPCR using a BioRad iCycler, SsoFast EvaGreen Supermix (Biorad, 172-5204), and the mitochondria-specific primers: mito sense 5'-GACGTTAGGTCAAGGTGTAG-3' and mito antisense 5'-CAACTAAGCACTCTACTCTC-3'. All measurements were normalized to *GAPDH*: *GAPDH* sense 5'-GACCCCTTCATTGACCTCAAC-3', and *GAPDH* antisense 5'-CTTCTCCATGGTGGTGAAGA-3'. Each experiment was performed in triplicate and mtDNA release was expressed as the ratio of mtDNA enrichment in the post-treatment supernatant to post-treatment mitochondria samples.

Flow Cytometry

Mitochondria were isolated and treated with GSDMD and caspase-11 as described above. NADH (Sigma Aldrich, N8129-50MG; 2.5 μ M) and staining dyes were also added during treatment. To assess mitochondrial membrane potential (MMP), mitochondria were stained with the MMP-insensitive MitoTracker Green FM (Thermo Fisher, M7514; 1 μ M) and MMP dye MitoProbe DiIC1(5) (Thermo Fisher, M34151; 50 nM) for 30 min at 37°C. CCCP (50 μ M) was used as a positive control. To assess ROS production, mitochondria were stained with the mitochondria-specific superoxide indicator MitoSox Red (Thermo Fisher, M26008, 5 μ M) for 30 min at 37°C, and antimycin A (Sigma Aldrich, A8674; 5 μ M) was used as a positive control. Mitochondria were analyzed using a FACSCanto II (BD Bioscience). Gating and identification of mitochondria was done according to Lecoeur *et al.* (64).

Fixed Cell Confocal Imaging

THP-1 cells (1.5×10^5 cells/well) were seeded and differentiated in Nunc Lab-Tek Chamber Slides (Thermo Fisher, 177402). Cells were primed with LPS and stained with the MMP-insensitive MitoTracker Deep Red FM (Thermo Fisher, M22426; 500 nM, 30 min, 37°C). Cells were induced to undergo pyroptosis

for indicated times at 37°C using nigericin. For intracellular staining, cells were fixed (4% paraformaldehyde, 10 min, RT), permeabilized (0.5% Triton-X 100 in PBS; 10 min, RT) and blocked (5% BSA in FACS Buffer; 30 min, RT) before incubating overnight at 4°C with antibodies to Cyt c (BioLegend, 612504, 1:1000), GSDMD (lab-generated, 1:100) or an isotype mouse IgG primary antibody (BioLegend, 40024; 1:100). This was followed by incubation with an Alexa Fluor 568-conjugated goat anti-mouse secondary antibody (Invitrogen, A-11031; 1:1000, 1 hr, RT) and Hoechst 33342 (Thermo Fisher, 62249; 1:100,000, 10 min, RT). Between all steps, cells were washed with FACS buffer (2 min, RT). Cover slips were applied using fluorescent mounting medium (Dako, S3023). Cells were imaged using a Zeiss 880 laser scanning confocal microscope at 63x magnification. Images were analyzed using Zeiss Zen software to assess colocalization of Cyt C or GSDMD with mitochondria.

Live Cell Confocal Imaging

THP-1 cells (1×10^5 cells) were seeded and differentiated in 35 mm imaging dishes (MatTek, p35g-1.5-10-c). Cells were stained with MitoSox Red (500 nM) and Mitotracker Deep Red FM (500 nM) for 30 min at 37°C, before SYTOX Green (200 nM) was added to cell media. Pyroptosis was induced using nigericin. Cells were imaged in a heated chamber (37°C, 5% CO₂) on a Zeiss 880 laser scanning confocal microscope at 63x magnification and analyzed using Zeiss Zen software. Kinetic analysis of single cells was performed according to sequential measurements of MitoSox Red, Mitotracker Deep Red FM and SYTOX Green signal intensity. To synchronize analysis of individual cells, timing was normalized to the first detection of SYTOX Green uptake. Signal intensity for each cell was quantified relative to the maximum intensity observed for a given dye during the sequence of analysis.

Electron Microscopy

THP-1 cells were seeded, differentiated, primed and treated with nigericin as described above. After indicated times, cells were fixed (2.5% paraformaldehyde, 2.5% glutaraldehyde, 0.05% picric acid in 0.2 M cacodylate buffer) for at least 2 hours, washed in 0.1 M cacodylate buffer, post-fixed (1% osmium tetroxide, 1.5% potassium ferrocyanide) for 1 hour, washed twice in water, once in maleate buffer (MB) and incubated in 1% uranyl acetate in MB for 1 hr. This was followed by 2 washes in water and subsequent dehydration in alcohol (10 min each; 50%, 70%, 90%, 2x 100%). The samples were then placed in propylene oxide for 1 hr and infiltrated in a 1:1 mixture of propylene oxide and TAAB Epon (TAAB Laboratories Equipment Ltd., T004). The following day samples were embedded in TAAB Epon and polymerized at 60°C for 48 hrs. 60 mm sections were cut on a Reichert Ultracut-S microtome and placed onto copper grids stained with lead citrate and examined using a TecnaiG² Spirit BioTWIN electron microscope. Images were recorded with an AMT 2k CCD camera at 3,000 and 10,000x magnification.

Microplate Reader Assays

PMA-treated THP-1 cells or iBMDMs (1×10^5 cells/well) were seeded in 96-well flat-bottom plates. Cells were primed with LPS and treated with either nigericin (20 μ M) or ATP (5 mM). All kinetic readings (2.5 min intervals, 45 min endpoint, 37°C) were performed using a Synergy H4 Hybrid Multi-Mode Microplate Reader (BioTek). To measure plasma membrane permeabilization during pyroptosis, SYTOX Green (1 μ M) was added to each well, and readings were performed at excitation/emission wavelengths of 485/528 nm. 0.02% Triton X-100 was used as a positive control. Assessment of MMP was performed using the JC-1 Mitochondrial Membrane Potential Assay Kit (Abcam, ab113850) according to supplier instructions. Readings were performed at excitation/emission wavelengths of 485/528 nm for JC-1 monomer and 485/620 nm for JC-1 aggregate. FCCP (5 μ M) was used as a positive control. Readings were analyzed as the ratio of aggregate to monomer emission. To assess ROS production, a DCFDA Cellular ROS

Assay Kit, (Abcam, ab113861) was used according to supplier instructions. Readings were performed at excitation/emission wavelengths of 485/528 nm. Tert-butyl hydrogen peroxide (TBHP; 50 μ M) was used as a positive control for ROS production. All plate reader experiments were performed in triplicate.

Pyroptotic Cell Fractionation Assay

THP-1 cells (7.5×10^6 cells/group) were differentiated and primed with LPS as described above. Cells were then detached using 0.25% Trypsin-EDTA (Thermo Fisher, 25200056) and resuspended in PBS. Pyroptosis was induced using nigericin for indicated times and subsequently pelleted (850 xg, 4°C, 2 min). After a culture supernatant sample was collected, cell pellets were resuspended in isotonic Buffer A and fractionated to obtain cytosol and mitochondria fractions as described above. Western blots were used to probe the cell supernatant, cytosol and mitochondria fractions for indicated proteins.

siRNA Knockdown

iBMDMs were transfected with siRNA using the Amaxa Mouse Nucleofection Kit (Lonza Bioscience) according to the supplier instructions. iBMDMs (1×10^6) were transfected with siRNA (50 nM) targeting *Crls1* (Thermo Fisher, s83501 & s83502) or *Plscr3* (Thermo Fisher, s88686 & s88688). siRNA knockdown was confirmed 48 hrs later by qPCR, using a BioRad iCycler, SsoFast EvaGreen Supermix, and *Crls1* (sense 5'-GCCAGCTCGTATGAAAATCCA-3', antisense 5'-GCAAAAACACCTAGTGCAACATT-3') or *Plscr3*-specific primers (sense 5'-CCTGCTCCTTTCGTGCCATT-3', antisense 5'-CGTTTCCACTCGTTCAGCCT-3'). mRNA abundance was normalized to *GAPDH* (sense 5'-GACCCCTTCATTGACCTCAAC-3', antisense 5'-CTTCTCCATGGTGGTGAAGA-3'). Each sample was measured in triplicate.

48 hrs after siRNA transfection, iBMDMs were treated with LPS and nigericin to undergo pyroptosis. Cell death was measured using the lactate dehydrogenase (LDH) release assay and analyzed as the

percentage of dead cells, inferred from the maximum reading of the positive control (0.02% Triton-X100). Each measurement was performed in triplicate.

Statistical Analysis

All data is presented as mean \pm SD and was analyzed using the student paired t-test, one-way ANOVA or two-way ANOVA. Statistical analysis was performed using GraphPad Prism software (version 6.0).

Chapter Three: Results

GSDMD-NT binds to and permeabilizes isolated mitochondria.

Given that GSDMD-NT can bind to cardiolipin, a phospholipid found on mitochondrial membranes, we first investigated whether GSDMD-NT could bind to and permeabilize mitochondrial membranes in a cell-free model. When mitochondria isolated from HCT116 cells were treated with recombinant GSDMD and caspase-11, soluble mitochondrial proteins from the IMS (Cyt c and HtrA2) and matrix (Aco2 and SOD2) were released (Fig. 5A-C) (65, 66). Protein release did not occur when GSDMD or caspase-11 was absent, or when the pan-caspase inhibitor Z-VAD-FMK was given, confirming permeabilization was mediated by GSDMD-NT. Furthermore, treatment with t-Bid only permeabilized the OMM as expected. Together these findings show that GSDMD-NT can bind to mitochondria and uniquely permeabilize both the OMM and IMM. To further investigate the kinetics of this permeabilization, time-course assays demonstrated that GSDMD-NT rapidly permeabilizes the OMM and IMM, as Cyt c and Aco2 were both released within 5 min (Fig. 5C). Observing the release of mitochondrial proteins made us wonder if other mitochondrial molecules are released by GSDMD-NT. Indeed, probing for mtDNA with qPCR showed that GSDMD and caspase-11 treatment mediated mtDNA release from mitochondria (Fig. 5D).

GSDMD-NT permeabilization of isolated mitochondria increases mitochondrial ROS production and lowers mitochondrial trans-membrane potential

In apoptosis, permeabilization of mitochondria by pro-apoptotic factors causes organelle dysfunction characterized by increased ROS production and loss of mitochondrial trans-membrane potential (MMP) (63). Therefore, we investigated whether GSDMD-NT permeabilization of mitochondria causes similar outcomes. Flow cytometry of isolated mitochondria, stained with the mitochondria superoxide indicator MitoSox Red or MMP indicator MitoProbe DiIC1(5), showed that GSDMD and caspase-11 treatment caused significantly elevated ROS production and reduced MMP (Fig. 6).

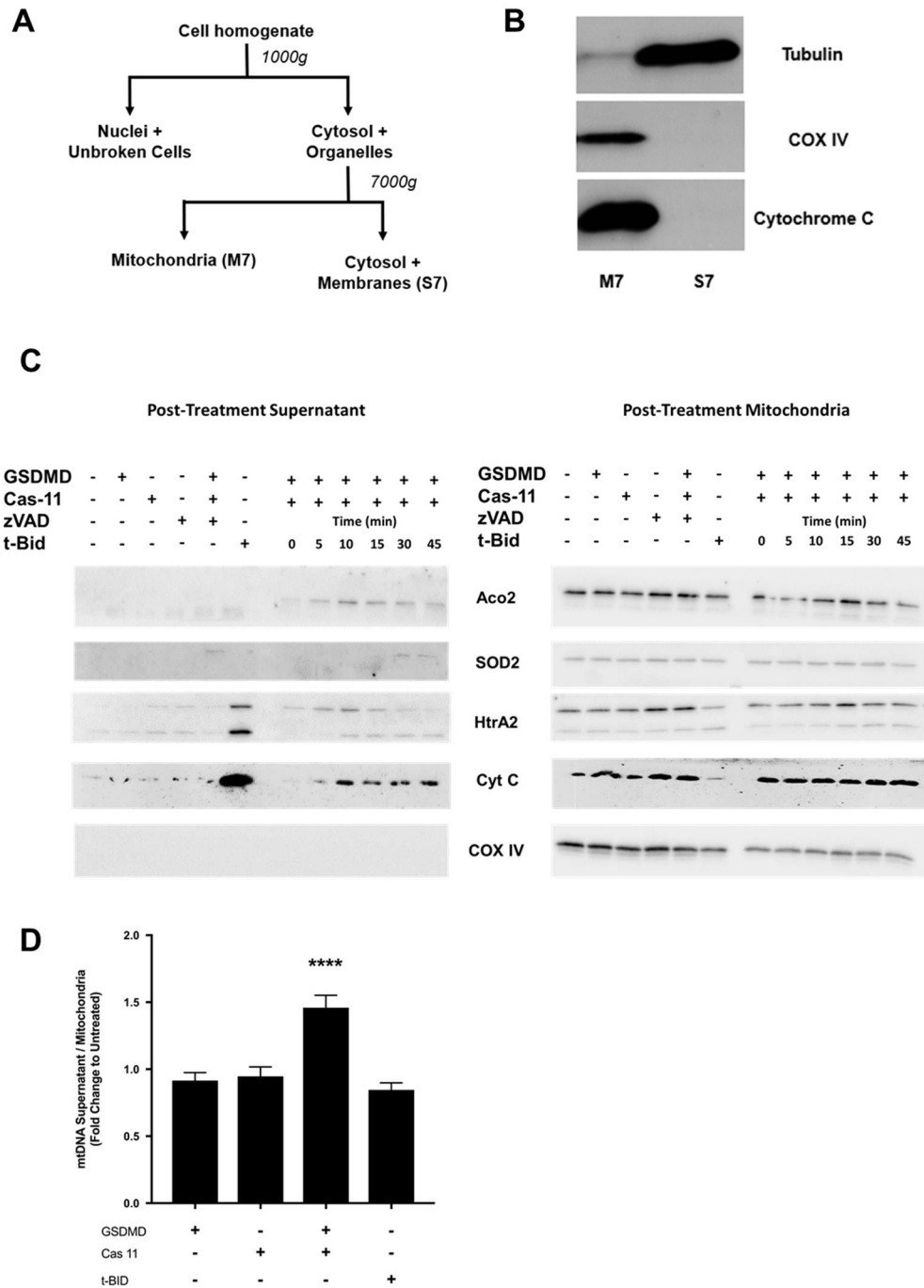


Figure 5. GSDMD-NT permeabilizes the OMM and IMM. (A, B) Mitochondria (M7) were isolated from HCT116 cells using cell fractionation. (C) Isolated mitochondria were treated with recombinant GSDMD and caspase 11 for indicated times. Post-treatment supernatant and mitochondria were probed for IMS proteins Cyt c and HtrA2, and matrix proteins ACO2 and SOD2 using Western blots. Pan-caspase inhibitor Z-VAD-FMK was used to inhibit GSDMD cleavage. T-Bid was used as a biological control. All control treatments lasted 45 min. The blot shown is representative of three independent experiments. (D) MtDNA was probed from post-treatment supernatant and mitochondria samples using qPCR. MtDNA release was measured as the ratio of enrichment in post-treatment supernatant to mitochondria. Data is presented as mean \pm SD of three independent experiments and analyzed using two-way ANOVA. **** $p < 0.0001$.

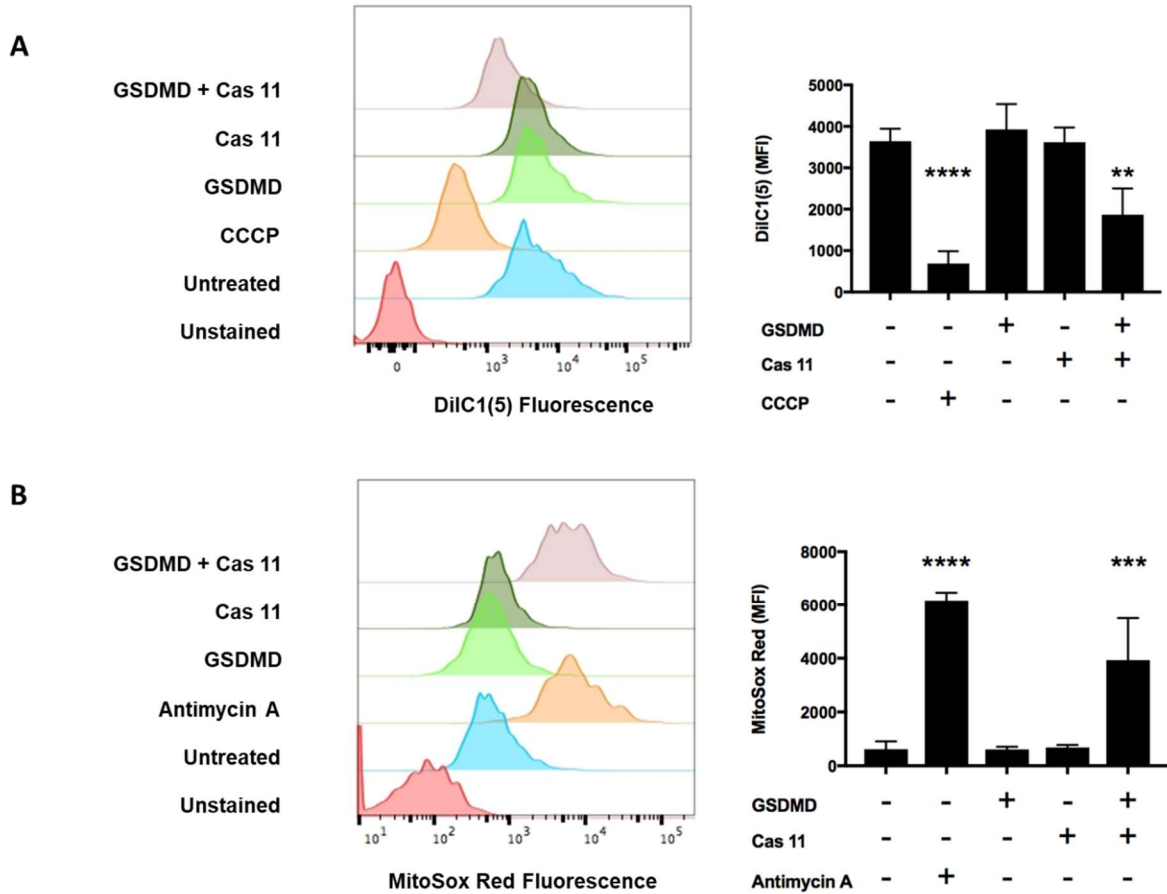


Figure 6. GSDMD-NT permeabilization of mitochondria leads to increased ROS production and reduced MMP. Isolated mitochondria were treated with recombinant human GSDMD and caspase 11 for 45 min. Mitochondria were stained with (A) MitoProbe DiIC1(5) or (B) MitoSox Red and assessed using flow cytometry. CCCP and antimycin A were used as positive controls for MMP and ROS, respectively. Data is presented as mean \pm SD of at least three independent experiments and analyzed using one-way ANOVA. ** $p < 0.01$. *** $p < 0.001$. **** $p < 0.0001$.

GSDMD-NT binds to mitochondria and mitochondrial proteins are released during pyroptosis.

To validate our findings using isolated mitochondria, we turned to *in vitro* studies of THP-1 cells. To induce pyroptosis, THP-1 cells were treated with LPS and nigericin, which triggers the NLRP3-mediated canonical pathway. To determine whether GSDMD-NT binds to mitochondria during pyroptosis, we performed immunofluorescence (IF) confocal microscopy of GSDMD during pyroptosis to observe colocalization with mitochondria labeled with the MMP-insensitive dye MitoTracker Deep Red FM (MTDR) (Fig. 7). As expected, GSDMD was distributed throughout the cytosol with minimal colocalization to mitochondria in the absence of pyroptosis. However, after nigericin treatment, GSDMD rapidly colocalized with mitochondria within 5 min. This colocalization began to diminish 15-30 min after nigericin treatment, and was associated with migration of GSDMD to the plasma membrane at 30 min. We also performed IF confocal microscopy of Cyt c-mitochondria colocalization to assess mitochondrial protein release during pyroptosis (Fig. 8). Prior to pyroptosis, Cyt c had strong colocalization with MTDR. Nigericin treatment caused gradual release of Cyt c, indicated by reduced colocalization to MTDR until 30 min (Fig. 8). As a result, our IF confocal microscopy data confirms that GSDMD-NT binding and mitochondrial protein release occur in pyroptosis.

We also probed subcellular fractions of pyroptotic THP-1 cells (Fig. 9). Western blots of the cytosolic fraction showed the appearance of activated caspase-1 (p20 fragment) at the onset of pyroptosis. This was matched with GSDMD and pro-IL-1 β cleavage 7.5 min after nigericin treatment. Furthermore, THP-1 cells showed gradual release of Cyt c and Aco2 from mitochondria into the cytosol during pyroptosis. Another interesting observation was caspase-3 activation (p20/p17 fragments) beginning 30 min after nigericin treatment, a known late-stage phenomenon in pyroptosis. The activation of caspase-1, GSDMD cleavage and mitochondrial protein release all began prior to cytosolic release of proteins into the culture

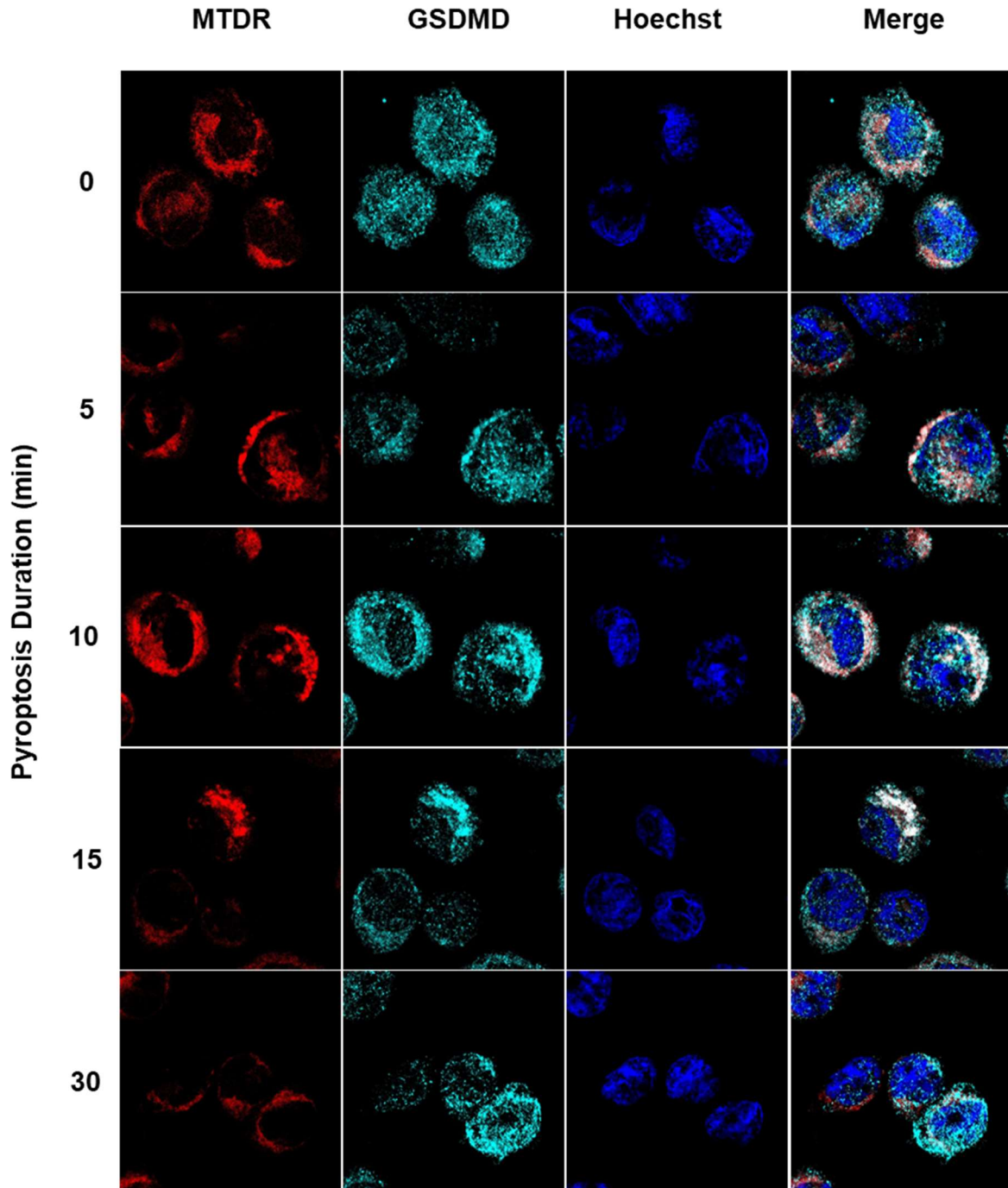


Figure 7. GSDMD-NT localizes to mitochondria early in pyroptosis. THP-1 cells were treated with LPS and nigericin to induce pyroptosis for indicated times. Cells were labelled with Hoechst 3342 (blue), MitoTracker Deep Red FM (MTDR; red) and stained for GSDMD (turquoise). Colocalization of GSDMD and mitochondria is indicated in white. Representative images were taken at 63x magnification under IF confocal microscopy.

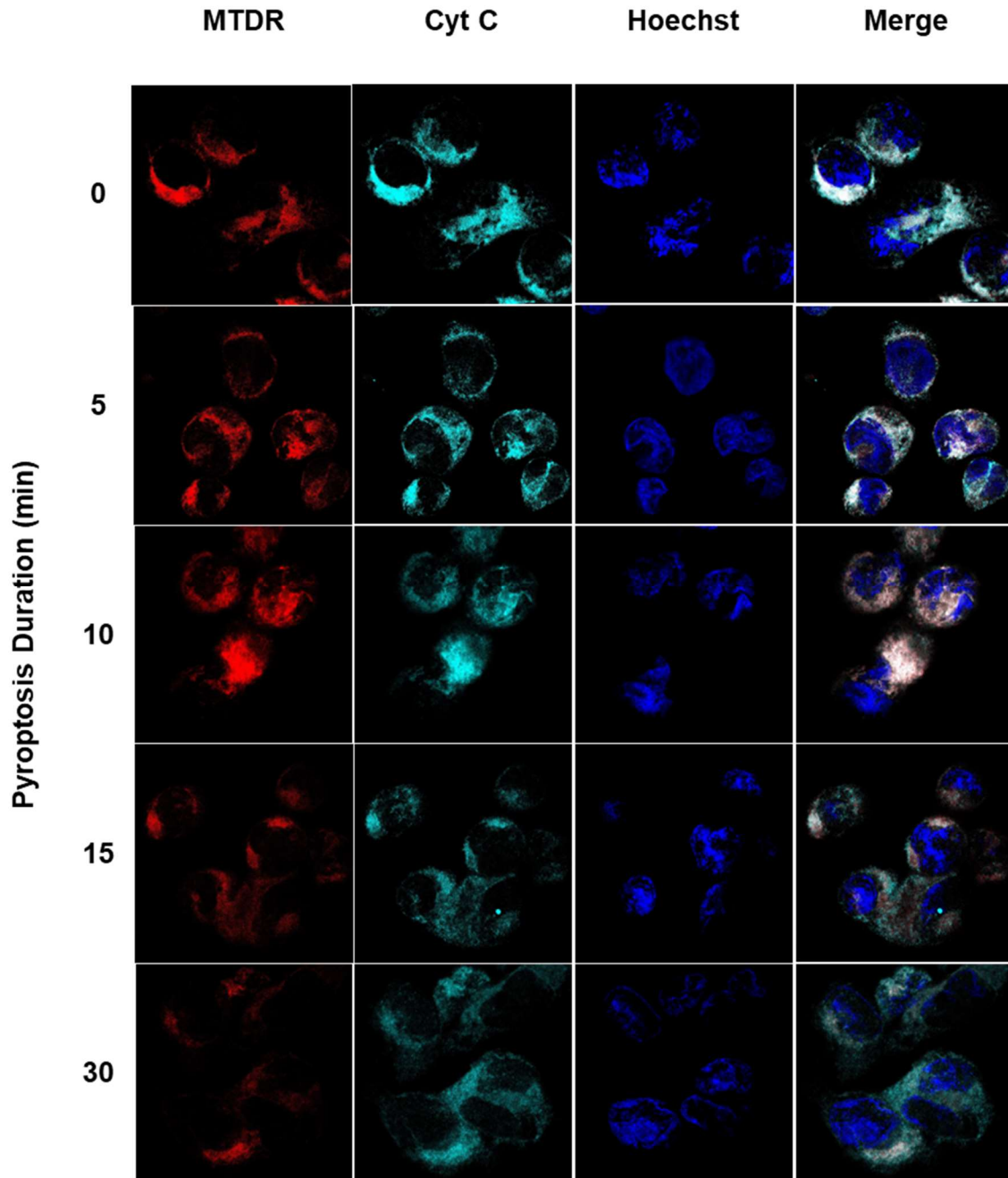


Figure 8. Cyt c is released from mitochondria during pyroptosis. THP-1 cells were treated with LPS and nigericin to induce pyroptosis for indicated times. Cells were labelled with Hoechst 3342 (blue), MitoTracker Deep Red FM (MTDR; red) and stained for Cyt c (turquoise). Colocalization of Cyt c and mitochondria is indicated in white. Representative images were taken at 63x magnification under IF confocal microscopy.

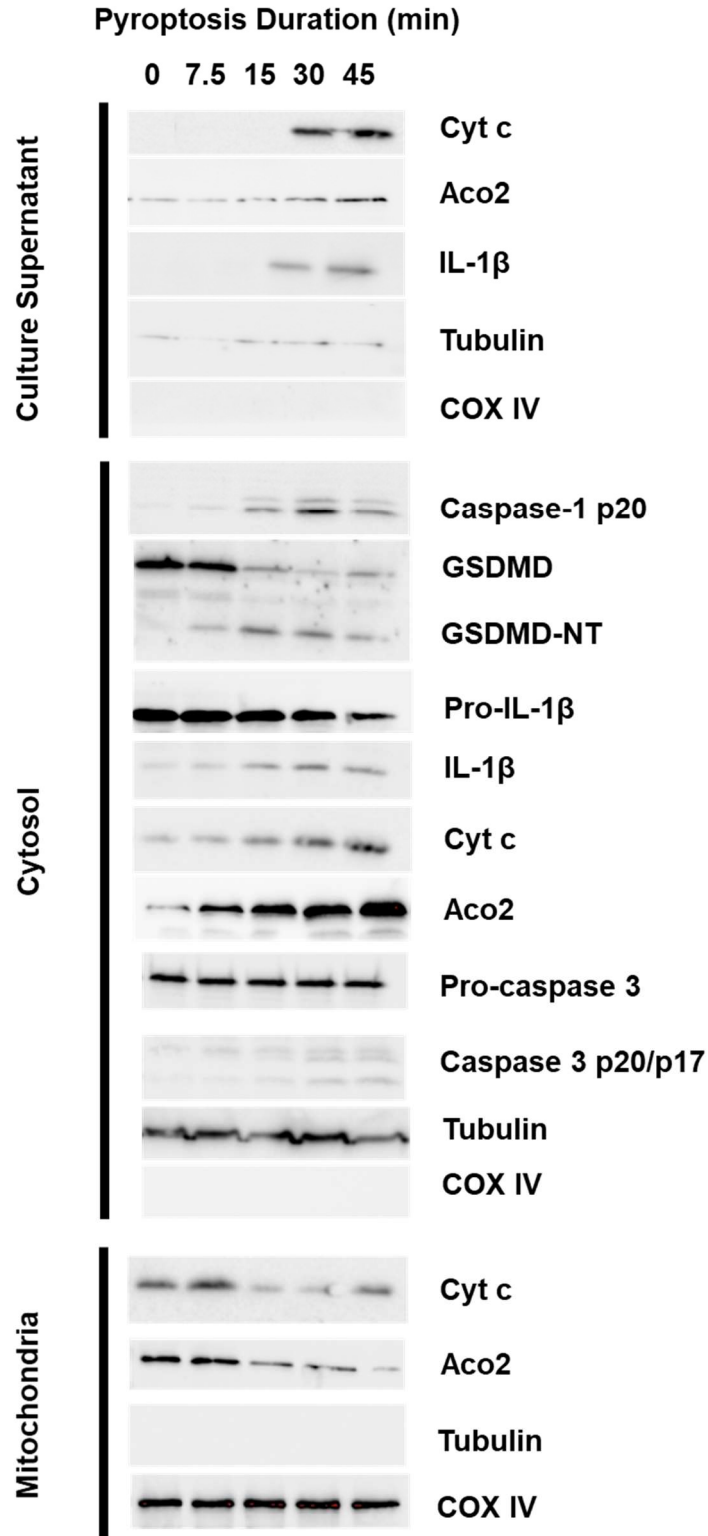


Figure 9. Caspase activation, GSDMD cleavage, and mitochondrial protein release are sequential. THP-1 cells were treated with LPS and nigericin to induce pyroptosis for indicated times. Cells were subsequently fractionated to collect culture supernatant, cytosolic and mitochondria fractions, which were probed for indicated proteins by Western blot. The blot shown is representative of three independent experiments.

supernatant which indicated GSDMD-NT permeabilization of the plasma membrane. Together, our IF confocal microscopy and subcellular fractionations suggest that GSDMD binding to mitochondria, permeabilization of OMM and IMM, and release of mitochondrial proteins occur early in pyroptosis, prior to GSDMD-NT's known role at the plasma membrane.

Pyroptosis results in structural damage and dissolution of mitochondria.

During our IF confocal microscopy of GSDMD and Cyt C in pyroptotic THP-1 cells, we unexpectedly observed the gradual loss of MTDR signal towards 30 min (Fig. 7 & 8). Given that MTDR is an MMP-insensitive dye, we postulated that the loss of staining could be linked to mitochondrial damage and dissolution. To evaluate mitochondrion morphology, we performed electron microscopy (EM) of pyroptotic THP-1 cells at indicated times (Fig. 10). While untreated THP-1 cells exhibited healthy mitochondria, observations at 30 min showed swelling and loss of cristae structure, hallmarks of mitochondria damage during cell death (63, 67). Mitochondrial damage continued to worsen, as observed at 60 min. Therefore, it is likely that the loss of MTDR signal is associated with mitochondrial damage. Given that GSDMD-NT binding of mitochondria and mitochondrial protein release occur during the loss of MTDR, it is possible that these mitochondrial events are connected.

Mitochondrial dysfunction occurs early in pyroptosis.

As GSDMD-NT binds to mitochondria early in pyroptosis, and data from isolated mitochondria suggested that binding leads to elevated ROS and reduced MMP, we investigated whether mitochondrial dysfunction also occurs early in pyroptosis (Fig. 6). Analysis of individual cells using live-cell IF confocal microscopy indicated that mitochondrial dissolution and elevated mitochondrial ROS production precede GSDMD-NT permeabilization of the plasma membrane, according to staining with MTDR, mitochondrial ROS indicator MitoSox Red and plasma membrane permeability indicator SYTOX Green (Fig. 11).

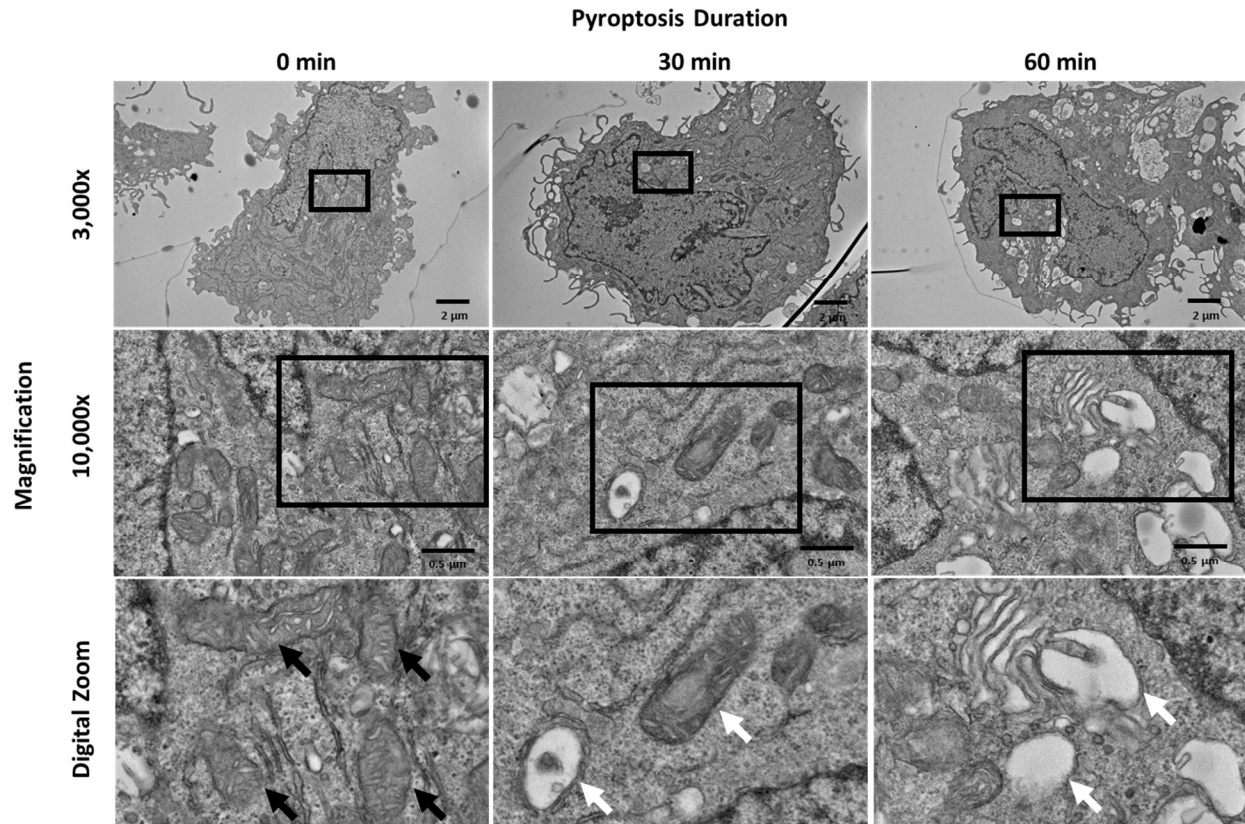
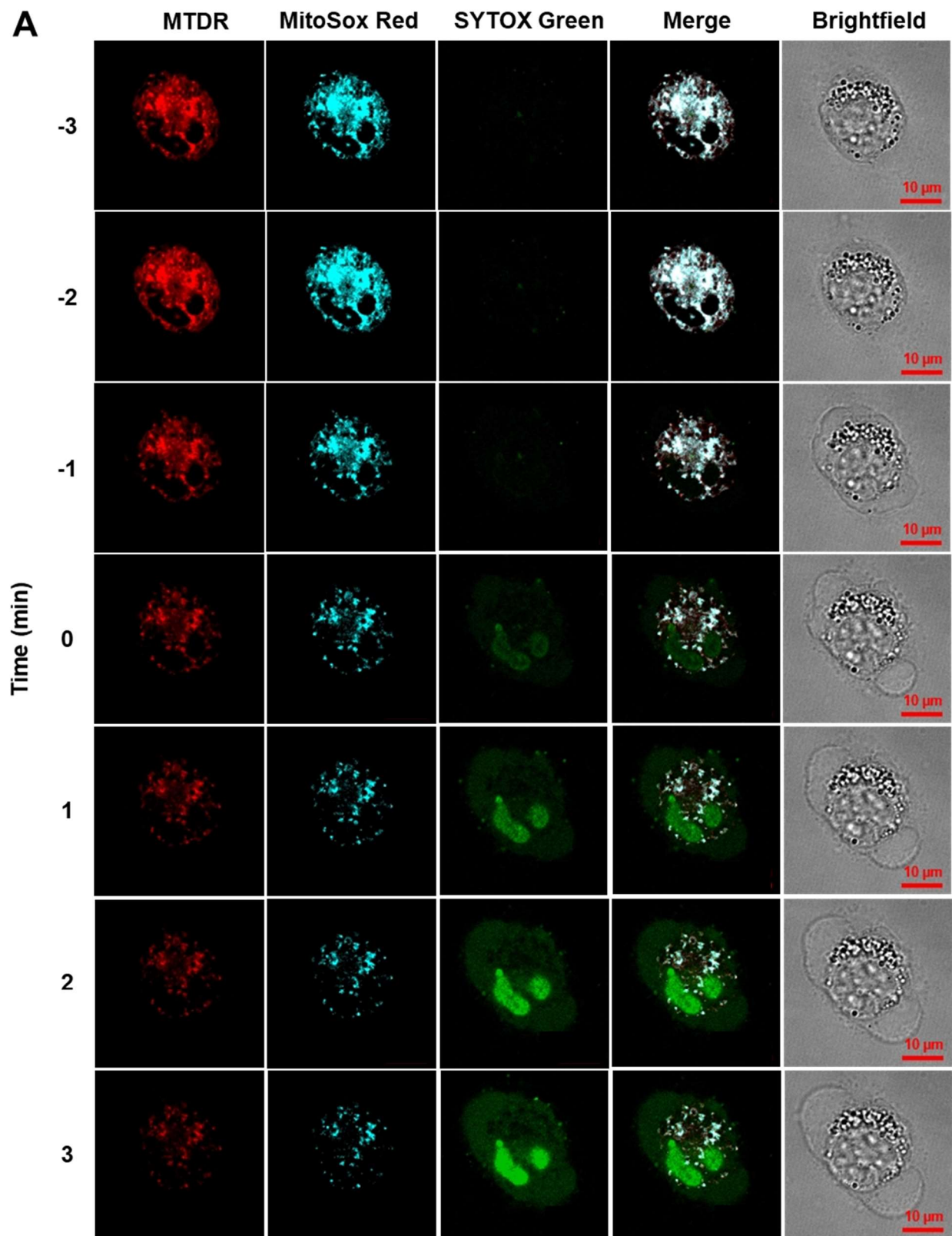


Figure 10. Mitochondria are structurally damaged in pyroptotic cells. THP-1 cells were treated with LPS and nigericin to induce pyroptosis for indicated times. Cells were then processed and imaged under electron microscopy. Representative images were taken at 3,000 and 10,000x magnification, followed by digital magnification. Black arrows indicate healthy mitochondria, while white arrows indicate mitochondrial swelling or loss of cristae.



(Figure 11A. See figure legend on next page)

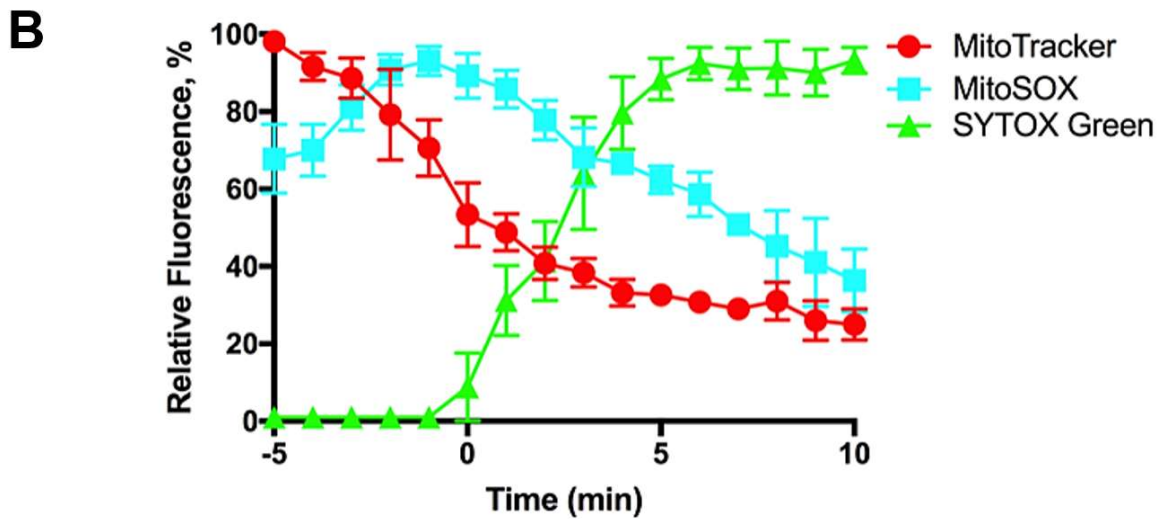


Figure 11 Mitochondrial dysfunction and dissolution occur prior to plasma membrane permeabilization in individual pyroptotic cells. THP-1 cells were treated with LPS and nigericin to induce pyroptosis. Cells were stained with MitoTracker Deep Red FM, MitoSox Red and SYTOX Green. (A) Pyroptotic cells were observed under live-cell IF confocal microscopy and (B) sequential measurements of signal intensity were performed for individual cells. Quantification of each cell was normalized kinetically to the moment of GSDMD-NT permeabilization of the plasma membrane, indicated by SYTOX Green uptake (Time 0). Signal intensity was quantified relative to the maximum intensity observed for a given dye during the analysis. Data is presented as mean \pm SD of ten cells.

Population-level assessment of pyroptotic cells by microplate readings of cellular ROS indicator DCF, MMP indicator JC-1 and SYTOX Green showed similar kinetics (Fig. 12). Pyroptotic THP-1 cells had a significant increase in cellular ROS beginning at 5 min and drop in MMP beginning at 15 min, while plasma membrane permeabilization started at 22.5 min after nigericin treatment. Microplate readings of iBMDMs undergoing NLRP3-mediated pyroptosis with nigericin or ATP showed a similar sequence of events (Fig. 13).

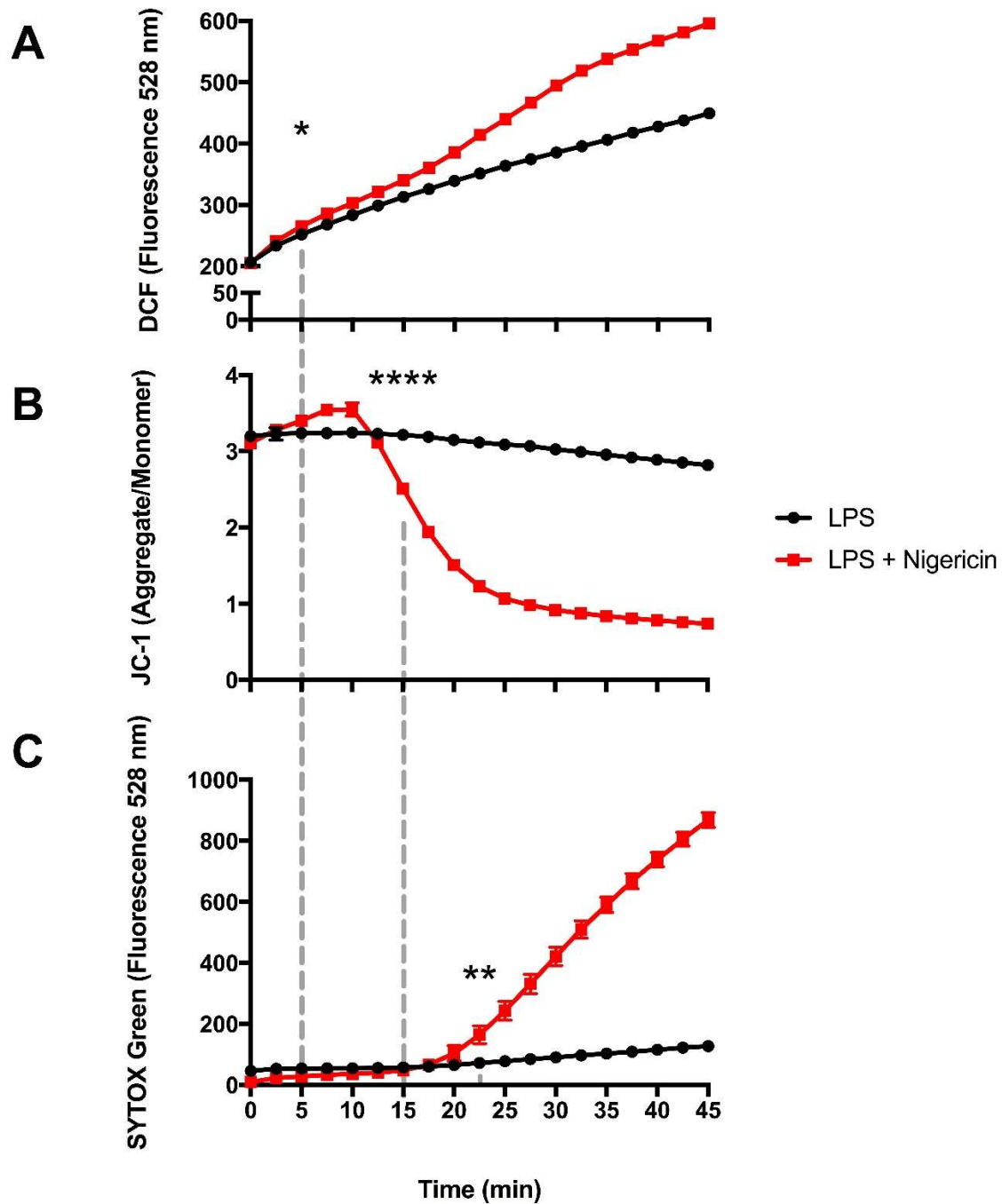


Figure 12. Mitochondrial dysfunction precedes plasma membrane permeabilization in pyroptotic THP-1 cell populations. THP-1 cells were stained with (A) DCF, (B) JC-1 or (C) SYTOX Green to assess ROS production, MMP and plasma membrane permeabilization, respectively. TBHP (50 μ M), FCCP (5 μ M) and Triton X-100 (0.02%) were used as positive controls, respectively. THP-1 cells were treated with LPS and nigericin to induce pyroptosis. Cells were measured kinetically using a microplate reader at 2.5 min intervals for 45 min. Dashed lines indicate the sequence of significance across microplate measurements. Data is presented as mean \pm SD of three technical replicates, representative of three independent experiments. Data was analyzed using student parried t-tests at each time point. * p <0.05. ** p <0.01. **** p <0.0001.

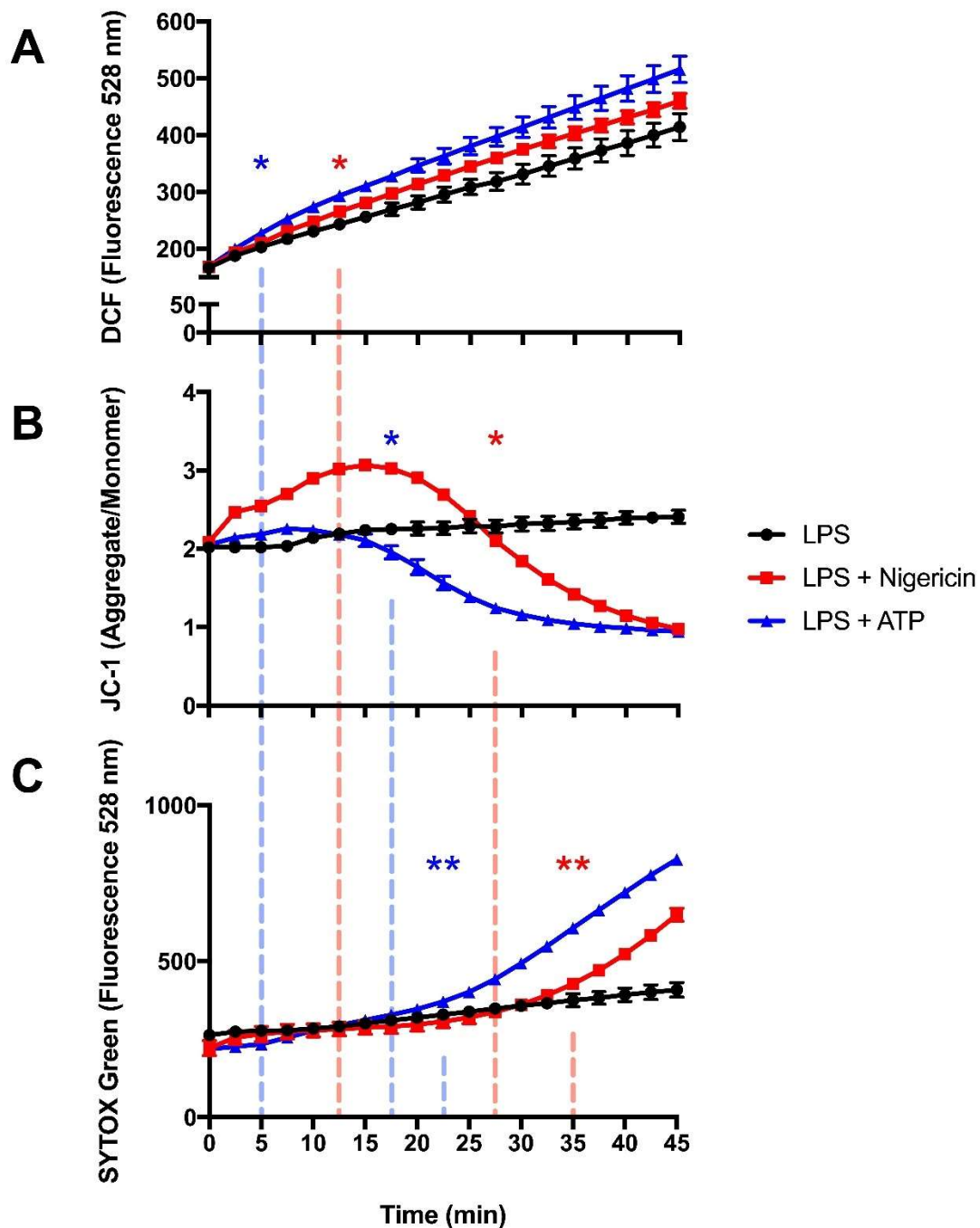


Figure 13. Mitochondrial dysfunction precedes plasma membrane permeabilization in pyroptotic iBMDM populations. iBMDMs were stained with (A) DCF, (B) JC-1 or (C) SYTOX Green to assess ROS production, MMP and plasma membrane permeabilization, respectively. TBHP (50 μ M), FCCP (5 μ M) and Triton X-100 (0.02%) were used as positive controls, respectively. iBMDMs were treated with LPS and either nigericin or ATP, to induce pyroptosis. Cells were measured kinetically using a microplate reader at 2.5 min intervals for 45 min. Dashed lines indicate the sequence of significance across microplate measurements. Data is presented as mean \pm SD of three technical replicates, representative of three independent experiments. Data was analyzed using student parried t-tests at each time point. * p <0.05. ** p <0.01.

Chapter Four: Discussion

GSDMD-NT's ability to form pores on membranes has sparked interest in the cellular locations where this protein functions during pyroptosis. Lipid binding assays have shown that GSDMD-NT can bind plasma membrane phospholipids necessary for cytosolic permeabilization (24). A greater affinity for cardiolipin, which is found in mitochondrial membranes, motivated our investigation of GSDMD-NT and mitochondria. Prior studies have suggested an association between GSDMD-NT and mitochondria. In an investigation of Shiga toxin-induced non-canonical pyroptosis, Platnich *et al.*, reported that secondary activation of NLRP3 inflammasomes was dependent on GSDMD-driven mitochondrial ROS production (68). Subcellular fractionation of Shiga toxin-treated THP-1 cells showed GSDMD-NT localization to the mitochondria fraction by immunoblotting. GSDMD KO THP-1 cells treated with Shiga toxin showed reduced mitochondrial ROS production. In another study using single-cell analysis, Vasconcelos *et al.*, documented mitochondrial disruption in BMDMs undergoing NLRP1- or NLRC4-mediated pyroptosis. Pyroptotic cells exhibited reduced fluorescence signal from MMP-sensitive MitoTracker Red and tetramethyl rhodamine (TMRM) (69). However, GSDMD KO BMDMs did not show reduced MMP. While both studies suggest a link between GSDMD-NT and mitochondria, it is uncertain whether the protein directly affects the organelle or colludes with additional molecules during pyroptosis. In this thesis, we show for the first time that GSDMD-NT can directly bind to mitochondria and permeabilize the OMM and IMM (Fig. 5). Permeabilization leads to the release of mitochondrial content, including soluble IMS/matrix proteins and mtDNA. In addition, GSDMD-NT binding leads to mitochondrial dysfunction with elevated ROS production and reduced MMP (Fig. 6). GSDMD-NT localization to mitochondria, the release of mitochondrial proteins and mitochondrial dysfunction all precede GSDMD-NT permeabilization of the plasma membrane in NLRP3-mediated pyroptotic THP-1 cells and iBMDMs, suggesting GSDMD-NT's role at mitochondria is an earlier event in pyroptosis (Fig. 7-13). This makes sense given GSDMD-NT's higher affinity for cardiolipin. Indeed, in their single cell analysis of pyroptotic BMDMs, Vasconcelos *et al.*, also report that reduced MMP occurs prior to

cells being stained by SYTOX Green (69). Our data supports this finding and highlights additional mitochondrial changes during early pyroptosis.

In this thesis, we do not show *in vitro* causality between GSDMD-NT binding to mitochondria, and the release of mitochondrial proteins or mitochondrial dysfunction. We plan to clarify this limitation by dissecting the interaction between GSDMD-NT and cardiolipin. While GSDMD-NT has affinity for cardiolipin, it is unconfirmed whether GSDMD-NT binding to mitochondria is dependent on cardiolipin. To investigate this question, we are knocking down (KD) the genes encoding cardiolipin synthase (CLS) and the mitochondrial scramblase PLS3 to reduce total cardiolipin and IMM-to-OMM externalization in mitochondria, respectively. Reduction in cardiolipin will be validated by confocal microscopy of cells stained with the cardiolipin-binding dye acridine orange 10-nonyl bromide (NAO). Preliminary studies in collaboration with Dr. Xing Liu have shown that siRNA KD of CLS and PLS3 in iBMDMs reduces NLRP3-mediated pyroptotic cell death (Fig. 14). However, it will also be critical to determine whether GSDMD localization to mitochondria is also reduced by siRNA KD during pyroptosis, validating GSDMD-NT's dependence on cardiolipin for its mitochondrial role. If this proves to be true, our siRNA KD strategy will be a useful tool to control GSDMD-NT binding to mitochondria without affecting the protein's other roles in pyroptosis. This will allow us to investigate whether inhibiting mitochondrial GSDMD-NT reduces or delays mitochondrial protein release and organelle dysfunction, establishing the causal link that we seek *in vitro*.

In our investigations of GSDMD-NT and mitochondria in pyroptosis, we utilized NLRP3-mediated models of pyroptosis (LPS plus nigericin; LPS plus ATP). It is necessary to evaluate our findings and future directions in other models of pyroptosis. These include the AIM2 model using poly dA:dT transfection, NAIP model using AP toxin and flagellin, and the non-canonical model using LPS transfection (70-73). These strategies will help establish GSDMD-NT binding to mitochondria as a general outcome in the molecular pathways of pyroptosis.

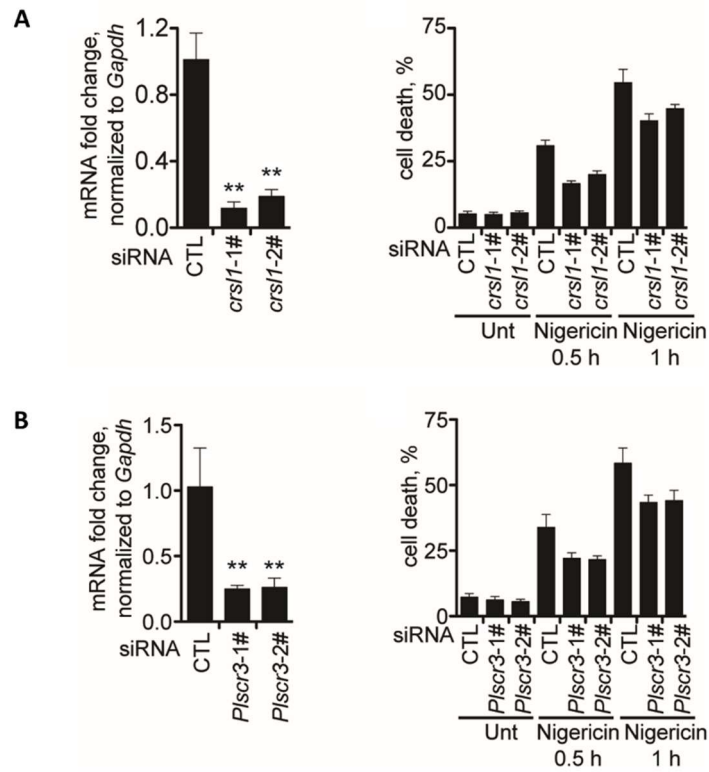


Figure 14. siRNA knockdown of cardiolipin synthase or PLS3 scramblase attenuates pyroptosis. iBMDMs were knocked down for (A) *crls1* or (B) *plscr3*. qPCR was performed to confirm siRNA knockdown. 48 hrs after siRNA transfection, iBMDMs were treated with LPS and nigericin to induce pyroptosis for indicated times. Cell viability was detected by LDH release assay.

The implications of GSDMD-NT binding to mitochondria during pyroptosis is an intriguing area of future investigation. We are especially interested in how the release of mitochondrial molecules, such as Cyt c and mtDNA, and elevated mitochondrial ROS interplay within pyroptosis (Fig. 5, 6). The cytosolic release of Cyt c is traditionally associated with classical apoptosis. Cytosolic Cyt c mediates formation of the APAF-1 apoptosome that activates caspase-9. Subsequently, caspase-9 cleaves and activates caspase-3 to execute apoptosis. In parallel, Cyt c release from GSDMD-NT permeabilization of mitochondria could activate caspase-3, which we observe in pyroptosis (Fig. 5, 8 & 9). Although caspase-3 activation in pyroptosis is well documented—an observation reported in the discovery of pyroptosis—the mechanism of activation remains poorly understood. Several studies have suggested that caspase-8, traditionally involved in the extrinsic pathway of apoptosis, may be involved (74-77). Canonical inflammasomes can recruit and activate caspase-1 to initiate pyroptosis. However, studies of the NLRP3 (nigericin), AIM2 (*Francisella novicia* infection) and NLRC4 inflammasomes (*Salmonella typhimurium* infection) report that caspase-8 can also be recruited and activated. This was shown by IF colocalization of pro-caspase-8 with ASC inflammasome specks in pyroptotic BMDM, loss of caspase-8 activation with NLRP3, AIM2, NLRC4 or ASC KO, and immunoprecipitation of caspase-8 with ASC (74-76). KO of inflammasome components and siRNA KD of caspase-8 reduced caspase-3 activation according to immunoblotting (75, 76). However, recent studies have shown that caspase-8 KO BMDMs still possess active caspase-3 in AIM2-mediated pyroptosis. Additional siRNA KD of caspase-1 in caspase-8 KO BMDMs further reduced caspase-3 activation (77). While the authors postulate that caspase-1 could directly cleave pro-caspase-3, a model in which caspase-1-generated GSDMD-NT permeabilizes mitochondria to release Cyt c should also be considered. This model may also serve as a broader mechanism for caspase-3 activation in both canonical and non-canonical pyroptosis. In addition to its mechanism of activation, caspase 3's biological purpose in pyroptosis is uncertain. Perhaps if downstream pathways of GSDMD-mediated pyroptosis are defective or inhibited by invading pathogens, caspase-3 can induce apoptosis to ensure removal of the infected cell. Caspase-3 is

also known to cleave GSDME, a gasdermin-related membrane pore-forming protein, to trigger secondary late-stage pyroptosis in apoptotic cells (78, 79). Similarly, if GSDMD-mediated pyroptosis fails in innate immune cells, caspase-3-GSDME pyroptosis could serve as a backup. Nonetheless, the activation of caspase-3 in pyroptosis and an increasing cross-talk between pyroptosis and apoptosis highlights the dynamism of cell death and the notion that dying cells are not governed by a fixed molecular pathway.

The cytosolic release of mtDNA after GSDMD-NT permeabilization of mitochondria could be detected by various DNA sensors that contribute to pyroptosis (Fig. 5D). MtDNA could bind to cGAS to trigger the anti-infection type-1 IFN response (T1-IFNR). Autocrine and paracrine signaling by IFN α/β during the T1-IFNR upregulates transcription of inflammasome sensors, inflammatory caspases and cytokine precursors. (80-82). Indeed P. West, *et al.*, have demonstrated this in a model of transcription factor A, mitochondrial (TFAM) deficiency. In the absence of TFAM, mtDNA is no longer packaged into nucleoids and escapes into the cytosol, according to qPCR of cytosolic subcellular fractions. The authors show that mtDNA localizes with cGAS to trigger the T1-IFNR, which is abrogated with cGAS KO (83). However, it has also been reported that mtDNA release in the context of apoptosis does not trigger the T1-IFNR due to poorly defined inhibitory functions of apoptotic caspases (84, 85). Indeed, these studies show that genetic KO or pharmacological inhibition of caspase-3/7/9 is necessary for mtDNA released via Bax/Bad pores to activate cGAS and the T1-IFNR. The authors believe that this inhibitory function of apoptotic caspases is necessary to ensure non-inflammatory cell death. However, whether mtDNA can trigger cGAS-mediated T1-IFNR in pyroptosis, and whether inflammatory caspases play an inhibitory role requires further investigation.

The release of mtDNA and elevated ROS production could also amplify activation of inflammasomes during pyroptosis. AIM2's role in detecting dsDNA could facilitate binding to mtDNA. In a study of 25 hydroxycholesterol hydrolase-deficient BMDMs, failure to metabolize cholesterol leads to a build-up that causes mitochondrial dysfunction and the release of mtDNA. This released mtDNA triggers

AIM2 inflammasome activation and inflammation (86). Furthermore, studies using the AIM2 *Francisella novicida* infection model suggest that GSDMD is crucial for optimal AIM2 and caspase-1 activation (87). While the dogma of canonical pyroptosis places GSDMD downstream of AIM2 and caspase-1, Zhu *et al.*, show that GSDMD KO iBMDMs have reduced caspase-1 activation according to immunoblotting. This could be rescued by endogenous expression of a retroviral vector containing GSDMD. It may be possible that GSDMD-NT permeabilization of mitochondria releases mtDNA that amplifies AIM2 and caspase-1 activation. In another interesting study in human monocytes, it was shown that cGAS-STING KO prevents dsDNA-induced pyroptosis. NLRP3 KO also prevented pyroptosis in human monocytes, suggesting a c-GAS-STING-NLRP3 axis. The authors demonstrated that cGAS-STING-dependent potassium efflux mediated NLRP3 activation. This suggests the possibility that cytosolic mtDNA can also trigger feed-forward activation through cGAS-STING and NLRP3. ROS is known to trigger NLRP3 activation, and given that mitochondrial ROS is elevated in pyroptosis, this may also amplify NLRP3 inflammasome activation (Fig 6, 11-13). Indeed, ROS associated with mitochondrial stress can be detected by NLRP3 and enhance susceptibility to cell death (88). Platnich *et al.*, suggest that GSDMD-NT permeabilization of mitochondrial membranes elevates mitochondrial ROS during Shiga toxin-induced non-canonical pyroptosis to trigger secondary activation of NLRP3. Given that GSDMD-NT is a common product of canonical and non-canonical pyroptosis, GSDMD-NT-induced mitochondrial ROS and activation of NLRP3 may serve as a broader amplification strategy across all pyroptotic pathways. Building on these ideas, it is intriguing to consider the breadth of secondary inflammasome activation caused by GSDMD-NT permeabilization of mitochondria. Are inflammasomes involved in amplification independent of the initiating inflammasome? Are certain inflammasomes more relevant to amplifying pyroptosis? Investigating these questions may require inhibitors of inflammasome sensors, such as MCC950 and A151 for NLRP3 and AIM2, respectively. Inhibition of mitochondrial molecules that may amplify inflammasome activation is also feasible. This includes using an inactive isoform of the DNA-sensor IF16- β for mtDNA, or treatment with antioxidants to neutralize mitochondrial ROS (89).

In conclusion, we show that GSDMD-NT binds to and permeabilizes mitochondria early in pyroptosis, leading to release of mitochondrial molecules like IMS/matrix proteins and mtDNA, and mitochondrial dysfunction with elevated ROS and loss of MMP. Given the wide-ranging possibilities for mitochondrial molecule release and ROS production to amplify pyroptosis and link alternate cell death programs, we propose that GSDMD-NT binding to mitochondria could mediate a mitochondrial cell death pathway, which contributes to pyroptosis (Fig. 15).

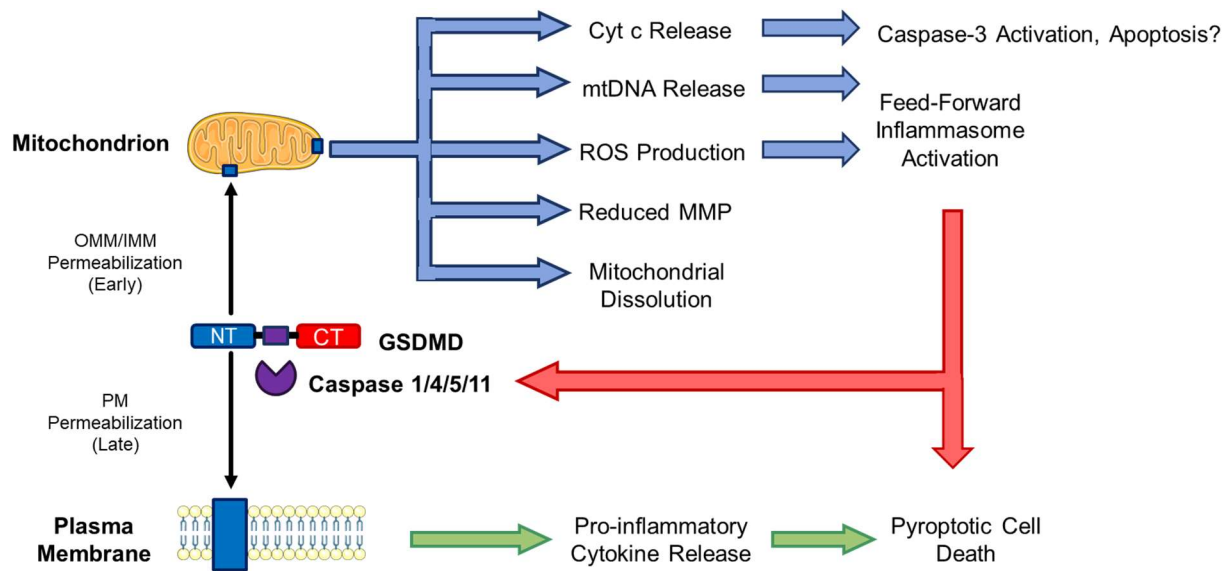


Figure 15. GSDMD-NT mediates a mitochondrial cell death pathway that contributes to pyroptosis. At the onset of pyroptosis, GSDMD is cleaved by inflammatory caspases to generate GSDMD-NT. GSDMD-NT's higher affinity for cardiolipin leads to early binding with mitochondria. This results in OMM/IMM permeabilization that damages the organelle, elevates ROS, lowers MMP and releases mitochondrial proteins and DNA. Release of Cyt c could activate caspase-3 to trigger apoptosis, while mtDNA and elevated ROS may amplify AIM2 and NLRP3 inflammasome activation. Later in pyroptosis, GSDMD-NT binds and permeabilizes the plasma membrane (PM), facilitating release of pro-inflammatory cytokines. It is likely that GSDMD-NT at the plasma membrane, mitochondria, and other undiscovered cellular locations participates in mediating pyroptotic cell death.

Bibliography

1. M. Lamkanfi, V. M. Dixit, Mechanisms and functions of inflammasomes. *Cell* **157**, 1013-1022 (2014).
2. L. M. Chen, K. Kaniga, J. E. Galán, Salmonella spp. are cytotoxic for cultured macrophages. *Mol Microbiol* **21**, 1101-1115 (1996).
3. S. W. Lindgren, I. Stojiljkovic, F. Heffron, Macrophage killing is an essential virulence mechanism of Salmonella typhimurium. *Proc Natl Acad Sci U S A* **93**, 4197-4201 (1996).
4. D. M. Monack, B. Raupach, A. E. Hromockyj, S. Falkow, Salmonella typhimurium invasion induces apoptosis in infected macrophages. *Proc Natl Acad Sci U S A* **93**, 9833-9838 (1996).
5. A. Zychlinsky, M. C. Prevost, P. J. Sansonetti, Shigella flexneri induces apoptosis in infected macrophages. *Nature* **358**, 167-169 (1992).
6. M. A. Brennan, B. T. Cookson, Salmonella induces macrophage death by caspase-1-dependent necrosis. *Mol Microbiol* **38**, 31-40 (2000).
7. Y. Chen, M. R. Smith, K. Thirumalai, A. Zychlinsky, A bacterial invasin induces macrophage apoptosis by binding directly to ICE. *EMBO J* **15**, 3853-3860 (1996).
8. C. M. Fernandez-Prada, D. L. Hoover, B. D. Tall, M. M. Venkatesan, Human monocyte-derived macrophages infected with virulent Shigella flexneri in vitro undergo a rapid cytolytic event similar to oncosis but not apoptosis. *Infect Immun* **65**, 1486-1496 (1997).
9. D. Hersh *et al.*, The Salmonella invasin SipB induces macrophage apoptosis by binding to caspase-1. *Proc Natl Acad Sci U S A* **96**, 2396-2401 (1999).
10. H. Hilbi *et al.*, Shigella-induced apoptosis is dependent on caspase-1 which binds to IpaB. *J Biol Chem* **273**, 32895-32900 (1998).
11. A. Zychlinsky, C. Fitting, J. M. Cavillon, P. J. Sansonetti, Interleukin 1 is released by murine macrophages during apoptosis induced by Shigella flexneri. *J Clin Invest* **94**, 1328-1332 (1994).
12. N. Kayagaki *et al.*, Caspase-11 cleaves gasdermin D for non-canonical inflammasome signalling. *Nature* **526**, 666-671 (2015).
13. J. Shi *et al.*, Cleavage of GSDMD by inflammatory caspases determines pyroptotic cell death. *Nature* **526**, 660-665 (2015).
14. K. Newton, G. Manning, Necroptosis and Inflammation. *Annu Rev Biochem* **85**, 743-763 (2016).
15. X. Chen *et al.*, Pyroptosis is driven by non-selective gasdermin-D pore and its morphology is different from MLKL channel-mediated necroptosis. *Cell Research* **26**, 1007-1020 (2016).
16. S. L. Fink, B. T. Cookson, Pyroptosis and host cell death responses during Salmonella infection. *Cell Microbiol* **9**, 2562-2570 (2007).
17. R. A. Aglietti, E. C. Dueber, Recent Insights into the Molecular Mechanisms Underlying Pyroptosis and Gasdermin Family Functions. *Trends Immunol* **38**, 261-271 (2017).
18. X. Liu, J. Lieberman, A Mechanistic Understanding of Pyroptosis: The Fiery Death Triggered by Invasive Infection. *Adv Immunol* **135**, 81-117 (2017).
19. M. Monteleone *et al.*, Interleukin-1 β Maturation Triggers Its Relocation to the Plasma Membrane for Gasdermin-D-Dependent and -Independent Secretion. *Cell Rep* **24**, 1425-1433 (2018).
20. N. J. Agard, D. Maltby, J. A. Wells, Inflammatory stimuli regulate caspase substrate profiles. *Mol Cell Proteomics* **9**, 880-893 (2010).
21. R. A. Aglietti *et al.*, GsdmD p30 elicited by caspase-11 during pyroptosis forms pores in membranes. *Proc Natl Acad Sci U S A* **113**, 7858-7863 (2016).
22. J. Ding *et al.*, Pore-forming activity and structural autoinhibition of the gasdermin family. *Nature* **535**, 111-116 (2016).

23. L. Sborgi *et al.*, GSDMD membrane pore formation constitutes the mechanism of pyroptotic cell death. *EMBO J* **35**, 1766-1778 (2016).
24. X. Liu *et al.*, Inflammasome-activated gasdermin D causes pyroptosis by forming membrane pores. *Nature* **535**, 153-+ (2016).
25. J. Ruan, S. Xia, X. Liu, J. Lieberman, H. Wu, Cryo-EM structure of the gasdermin A3 membrane pore. *Nature* **557**, 62-67 (2018).
26. E. Elinav *et al.*, NLRP6 inflammasome regulates colonic microbial ecology and risk for colitis. *Cell* **145**, 745-757 (2011).
27. D. Demon *et al.*, Caspase-11 is expressed in the colonic mucosa and protects against dextran sodium sulfate-induced colitis. *Mucosal Immunol* **7**, 1480-1491 (2014).
28. S. F. Yet, S. Lee, Y. T. Hahm, H. S. Sul, Expression and identification of p90 as the murine mitochondrial glycerol-3-phosphate acyltransferase. *Biochemistry* **32**, 9486-9491 (1993).
29. T. M. Lewin, N. M. Schwerbrock, D. P. Lee, R. A. Coleman, Identification of a new glycerol-3-phosphate acyltransferase isoenzyme, mtGPAT2, in mitochondria. *J Biol Chem* **279**, 13488-13495 (2004).
30. S. Wang *et al.*, Cloning and functional characterization of a novel mitochondrial N-ethylmaleimide-sensitive glycerol-3-phosphate acyltransferase (GPAT2). *Arch Biochem Biophys* **465**, 347-358 (2007).
31. Y. Q. Chen *et al.*, AGPAT6 is a novel microsomal glycerol-3-phosphate acyltransferase. *J Biol Chem* **283**, 10048-10057 (2008).
32. C. A. Nagle *et al.*, Identification of a novel sn-glycerol-3-phosphate acyltransferase isoform, GPAT4, as the enzyme deficient in *Agpat6*^{-/-} mice. *J Lipid Res* **49**, 823-831 (2008).
33. Y. Tamura *et al.*, Identification of Tam41 maintaining integrity of the TIM23 protein translocator complex in mitochondria. *J Cell Biol* **174**, 631-637 (2006).
34. Y. Tamura *et al.*, Tam41 is a CDP-diacylglycerol synthase required for cardiolipin biosynthesis in mitochondria. *Cell Metab* **17**, 709-718 (2013).
35. S. Kutik *et al.*, The translocator maintenance protein Tam41 is required for mitochondrial cardiolipin biosynthesis. *J Cell Biol* **183**, 1213-1221 (2008).
36. H. Cheng *et al.*, Shotgun lipidomics reveals the temporally dependent, highly diversified cardiolipin profile in the mammalian brain: temporally coordinated postnatal diversification of cardiolipin molecular species with neuronal remodeling. *Biochemistry* **47**, 5869-5880 (2008).
37. M. Schlame, S. Brody, K. Y. Hostetler, Mitochondrial cardiolipin in diverse eukaryotes. Comparison of biosynthetic reactions and molecular acyl species. *Eur J Biochem* **212**, 727-735 (1993).
38. S. C. Chang, P. N. Heacock, E. Mileykovskaya, D. R. Voelker, W. Dowhan, Isolation and characterization of the gene (CLS1) encoding cardiolipin synthase in *Saccharomyces cerevisiae*. *J Biol Chem* **273**, 14933-14941 (1998).
39. D. Chen, X. Y. Zhang, Y. Shi, Identification and functional characterization of hCLS1, a human cardiolipin synthase localized in mitochondria. *Biochem J* **398**, 169-176 (2006).
40. B. Lu *et al.*, Cloning and characterization of a cDNA encoding human cardiolipin synthase (hCLS1). *J Lipid Res* **47**, 1140-1145 (2006).
41. T. H. Haines, N. A. Dencher, Cardiolipin: a proton trap for oxidative phosphorylation. *FEBS Lett* **528**, 35-39 (2002).
42. D. Cheneval, M. Müller, E. Carafoli, The mitochondrial phosphate carrier reconstituted in liposomes is inhibited by doxorubicin. *FEBS Lett* **159**, 123-126 (1983).
43. K. Beyer, M. Klingenberg, ADP/ATP carrier protein from beef heart mitochondria has high amounts of tightly bound cardiolipin, as revealed by ³¹P nuclear magnetic resonance. *Biochemistry* **24**, 3821-3826 (1985).

44. K. S. Eble, W. B. Coleman, R. R. Hantgan, C. C. Cunningham, Tightly associated cardiolipin in the bovine heart mitochondrial ATP synthase as analyzed by ³¹P nuclear magnetic resonance spectroscopy. *J Biol Chem* **265**, 19434-19440 (1990).
45. K. Shinzawa-Itoh *et al.*, Structures and physiological roles of 13 integral lipids of bovine heart cytochrome c oxidase. *EMBO J* **26**, 1713-1725 (2007).
46. S. M. Claypool, Y. Oktay, P. Boonthueung, J. A. Loo, C. M. Koehler, Cardiolipin defines the interactome of the major ADP/ATP carrier protein of the mitochondrial inner membrane. *J Cell Biol* **182**, 937-950 (2008).
47. S. M. Claypool, Cardiolipin, a critical determinant of mitochondrial carrier protein assembly and function. *Biochim Biophys Acta* **1788**, 2059-2068 (2009).
48. C. T. Schwall, V. L. Greenwood, N. N. Alder, The stability and activity of respiratory Complex II is cardiolipin-dependent. *Biochim Biophys Acta* **1817**, 1588-1596 (2012).
49. H. Schägger, K. Pfeiffer, Supercomplexes in the respiratory chains of yeast and mammalian mitochondria. *EMBO J* **19**, 1777-1783 (2000).
50. Y. W. Lu, S. M. Claypool, Disorders of phospholipid metabolism: an emerging class of mitochondrial disease due to defects in nuclear genes. *Front Genet* **6**, 3 (2015).
51. M. Harner *et al.*, The mitochondrial contact site complex, a determinant of mitochondrial architecture. *EMBO J* **30**, 4356-4370 (2011).
52. K. von der Malsburg *et al.*, Dual role of mitofilin in mitochondrial membrane organization and protein biogenesis. *Dev Cell* **21**, 694-707 (2011).
53. Q. Zhou, P. J. Sims, T. Wiedmer, Identity of a conserved motif in phospholipid scramblase that is required for Ca²⁺-accelerated transbilayer movement of membrane phospholipids. *Biochemistry* **37**, 2356-2360 (1998).
54. J. Liu, J. Chen, Q. Dai, R. M. Lee, Phospholipid scramblase 3 is the mitochondrial target of protein kinase C delta-induced apoptosis. *Cancer Res* **63**, 1153-1156 (2003).
55. Q. Van *et al.*, Phospholipid scramblase-3 regulates cardiolipin de novo biosynthesis and its resynthesis in growing HeLa cells. *Biochem J* **401**, 103-109 (2007).
56. J. Liu *et al.*, Phospholipid scramblase 3 controls mitochondrial structure, function, and apoptotic response. *Mol Cancer Res* **1**, 892-902 (2003).
57. M. Tokarska-Schlattner *et al.*, The nucleoside diphosphate kinase D (NM23-H4) binds the inner mitochondrial membrane with high affinity to cardiolipin and couples nucleotide transfer with respiration. *J Biol Chem* **283**, 26198-26207 (2008).
58. T. Kuwana *et al.*, Bid, Bax, and lipids cooperate to form supramolecular openings in the outer mitochondrial membrane. *Cell* **111**, 331-342 (2002).
59. S. Lucken-Ardjomande, S. Montessuit, J. C. Martinou, Contributions to Bax insertion and oligomerization of lipids of the mitochondrial outer membrane. *Cell Death Differ* **15**, 929-937 (2008).
60. F. Gonzalez *et al.*, Cardiolipin provides an essential activating platform for caspase-8 on mitochondria. *J Cell Biol* **183**, 681-696 (2008).
61. L. Vande Walle, M. Lamkanfi, P. Vandenabeele, The mitochondrial serine protease HtrA2/Omi: an overview. *Cell Death Differ* **15**, 453-460 (2008).
62. K. McArthur *et al.*, BAK/BAX macropores facilitate mitochondrial herniation and mtDNA efflux during apoptosis. *Science* **359**, (2018).
63. G. Jacquemin *et al.*, Granzyme B-induced mitochondrial ROS are required for apoptosis. *Cell Death Differ* **22**, 862-874 (2015).
64. H. Lecoecur *et al.*, Real-time flow cytometry analysis of permeability transition in isolated mitochondria. *Exp Cell Res* **294**, 106-117 (2004).

65. M. Morgenstern *et al.*, Definition of a High-Confidence Mitochondrial Proteome at Quantitative Scale. *Cell Rep* **19**, 2836-2852 (2017).
66. F. N. Vögtle *et al.*, Landscape of submitochondrial protein distribution. *Nat Commun* **8**, 290 (2017).
67. R. Palchaudhuri *et al.*, A Small Molecule that Induces Intrinsic Pathway Apoptosis with Unparalleled Speed. *Cell Rep* **13**, 2027-2036 (2015).
68. J. M. Platnich *et al.*, Shiga Toxin/Lipopolysaccharide Activates Caspase-4 and Gasdermin D to Trigger Mitochondrial Reactive Oxygen Species Upstream of the NLRP3 Inflammasome. *Cell Reports* **25**, 1525-U1520 (2018).
69. N. M. de Vasconcelos, N. Van Opdenbosch, H. Van Gorp, E. Parthoens, M. Lamkanfi, Single-cell analysis of pyroptosis dynamics reveals conserved GSDMD-mediated subcellular events that precede plasma membrane rupture. *Cell Death Differ* **26**, 146-161 (2019).
70. J. Yang, Y. Zhao, J. Shi, F. Shao, Human NAIP and mouse NAIP1 recognize bacterial type III secretion needle protein for inflammasome activation. *Proc Natl Acad Sci U S A* **110**, 14408-14413 (2013).
71. J. Shi *et al.*, Inflammatory caspases are innate immune receptors for intracellular LPS. *Nature* **514**, 187-192 (2014).
72. H. Xu *et al.*, Innate immune sensing of bacterial modifications of Rho GTPases by the Pyrin inflammasome. *Nature* **513**, 237-241 (2014).
73. Z. Hu *et al.*, Antimicrobial cathelicidin peptide LL-37 inhibits the LPS/ATP-induced pyroptosis of macrophages by dual mechanism. *PLoS One* **9**, e85765 (2014).
74. S. M. Man *et al.*, Salmonella infection induces recruitment of Caspase-8 to the inflammasome to modulate IL-1 β production. *J Immunol* **191**, 5239-5246 (2013).
75. R. Pierini *et al.*, AIM2/ASC triggers caspase-8-dependent apoptosis in Francisella-infected caspase-1-deficient macrophages. *Cell Death Differ* **19**, 1709-1721 (2012).
76. V. Sagulenko *et al.*, AIM2 and NLRP3 inflammasomes activate both apoptotic and pyroptotic death pathways via ASC. *Cell Death Differ* **20**, 1149-1160 (2013).
77. V. Sagulenko, N. Vitak, P. R. Vajjhala, J. E. Vince, K. J. Stacey, Caspase-1 Is an Apical Caspase Leading to Caspase-3 Cleavage in the AIM2 Inflammasome Response, Independent of Caspase-8. *J Mol Biol* **430**, 238-247 (2018).
78. Y. Wang *et al.*, Chemotherapy drugs induce pyroptosis through caspase-3 cleavage of a gasdermin. *Nature* **547**, 99-103 (2017).
79. C. Rogers *et al.*, Cleavage of DFNA5 by caspase-3 during apoptosis mediates progression to secondary necrotic/pyroptotic cell death. *Nat Commun* **8**, 14128 (2017).
80. L. Franchi, R. Muñoz-Planillo, G. Núñez, Sensing and reacting to microbes through the inflammasomes. *Nat Immunol* **13**, 325-332 (2012).
81. P. K. Anand, R. K. Malireddi, T. D. Kanneganti, Role of the nlrp3 inflammasome in microbial infection. *Front Microbiol* **2**, 12 (2011).
82. R. K. Malireddi, T. D. Kanneganti, Role of type I interferons in inflammasome activation, cell death, and disease during microbial infection. *Front Cell Infect Microbiol* **3**, 77 (2013).
83. A. P. West, G. S. Shadel, S. Ghosh, Mitochondria in innate immune responses. *Nat Rev Immunol* **11**, 389-402 (2011).
84. A. Rongvaux *et al.*, Apoptotic caspases prevent the induction of type I interferons by mitochondrial DNA. *Cell* **159**, 1563-1577 (2014).
85. M. J. White *et al.*, Apoptotic caspases suppress mtDNA-induced STING-mediated type I IFN production. *Cell* **159**, 1549-1562 (2014).
86. E. V. Dang, J. G. McDonald, D. W. Russell, J. G. Cyster, Oxysterol Restraint of Cholesterol Synthesis Prevents AIM2 Inflammasome Activation. *Cell* **171**, 1057-1071.e1011 (2017).

87. Q. Zhu, M. Zheng, A. Balakrishnan, R. Karki, T. D. Kanneganti, Gasdermin D Promotes AIM2 Inflammasome Activation and Is Required for Host Protection against. *J Immunol* **201**, 3662-3668 (2018).
88. H. Luo *et al.*, Mitochondrial Stress-Initiated Aberrant Activation of the NLRP3 Inflammasome Regulates the Functional Deterioration of Hematopoietic Stem Cell Aging. *Cell Rep* **26**, 945-954.e944 (2019).
89. P. H. Wang *et al.*, Inhibition of AIM2 inflammasome activation by a novel transcript isoform of IFI16. *EMBO Rep* **19**, (2018).

Appendices

6.1 Author Contributions

The scientific work presented in this thesis was performed under the direction of Judy Lieberman, M.D., Ph.D., in the Program in Cellular and Molecular Medicine (PCMM) at Boston Children's Hospital, and in affiliation with the Master of Medical Sciences in Immunology Program at Harvard Medical School. Direct supervision was provided by Xing Liu, Ph.D, and Caroline Junqueira, Ph.D. All data shown in this thesis were generated by the author unless noted. Imaging and analysis for Fig. 7, 8, & 11 was performed by Caroline Junqueira. The data presented in Fig. 14 was generated by Xing Liu and his team at the Institute Pasteur of Shanghai – Chinese Academy of Sciences.